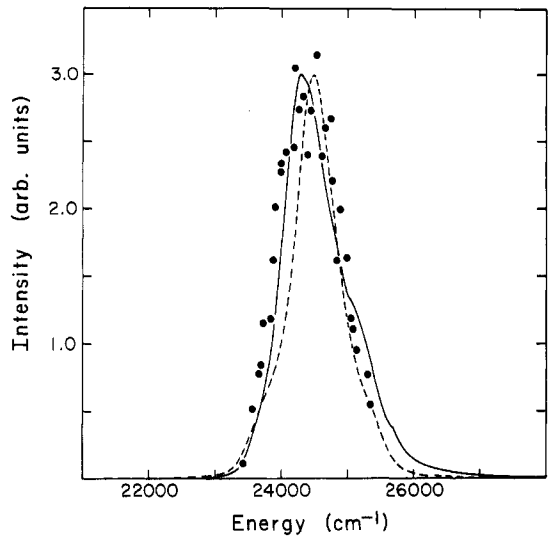

Figure 4. The experimental REP of the 690-cm^{-1} vibrational band of ferrocytochrome *c* at room temperature and the REP (solid curve) calculated by the forward transform of the solid curve in Figure 3b (C_a = −0.16). The dotted curve is the REP obtained by using the Condon approximation for *both* the inverse and the forward transforms.

absorption bands and in REP's.

Thermal effects can also lead to subtle errors in the transform/inverse transform technique. This problem has been recently discussed in detail by Chan and Page[10] where it is shown that negligible error results for systems having many "equivalent" weakly coupled low-frequency modes. Recent experimental studies of the Stokes and anti-Stokes Raman scattering of cytochrome *c*[11] also support the application of eq 1 and 2 at finite temperature when the optical features of the absorption band are diffuse ($\gtrsim kT$) and distinct progressions of the low-frequency subspace are not observed. As discussed previously,[3] care must be exercised when $T \neq 0$ K and a single low-frequency mode is strongly coupled to the transition (e.g. the transform and inverse transform of Figure 1c,d would contain significant error if $T \neq 0$ K). The general question of the quantitative importance of ensemble effects is receiving further attention.

In order to see whether the absorption band obtained by the inverse transform of the observed REP of one vibrational mode can be used to generate the REP of another vibrational mode, the REP of the 690-cm^{-1} vibrational mode of ferrocytochrome *c* is calculated by forward transforming the absorption band obtained from the inverse transform of the observed REP of the 1362-cm^{-1} mode (solid line in Figure 3b). The REP_{690} thus determined, but under different conditions, is presented in Figure 4 together with the experimentally observed one. Here again, it is found that to reach agreement the non-Condon effect as a parameter ($C_a \neq 0$) is essential both for the inverse transform of REP_{1362} (as we have seen by peak matching) and for the forward transform to produce the REP of the 690-cm^{-1} mode. This agrees well with previous work using the forward transform alone.[3]

Conclusion

A method is described which transforms an observed resonance Raman profile of a scattered vibration into the absorption band responsible for the scattering. The technique is applied to several examples, both model based and experimental, and it appears to be very successful in these few (but diverse) applications. The ultimate value of the method for resolving complex absorption bands into separate electronic transitions and for uncovering vibronic coupling parameters requires a much broader range of Raman profile data for testing.

Acknowledgment. This work was supported by grants from the National Science Foundation (CHE-80-16526) and the National Institutes of Health (AM-30714) and by the Materials Science Center of Cornell University.

(10) Chan, C. K.; Page, J. B. *J. Chem. Phys.* **1983**, *79*, 5234.
(11) Schomacker, K. T.; Bangcharoenpaurpong, O.; Champion, P. M. *J. Chem. Phys.* **1984**, *80*, 4701.

Lead Monoxide. Electronic Structure and Bonding

Georges Trinquier[†] and Roald Hoffmann*

Department of Chemistry, Cornell University, Ithaca, New York 14853 *(Received: April 17, 1984; In Final Form: September 10, 1984)*

The electronic structures of the two polymorphic forms of lead monoxide (PbO), red tetragonal α-PbO and yellow orthorhombic β-PbO, are investigated by using extended Hückel tight-binding calculations. The band structures and bonding are analyzed within the layers and also for the complete three-dimensional solids. In red α-PbO a local energy minimum is obtained when the layers are stacked together. For yellow β-PbO, the bonding is studied starting from PbO subunits and building successively chains, layers, and the three-dimensional solid. Bonding between chains occurs mainly through Pb–O but Pb–Pb bonding interactions are also significant. In both α and β modifications we find weak interlayer Pb–Pb bonding which we think is not the result of van der Waals attraction. Crystal orbital overlap populations provide a convenient view of the bonding in the two solids. Within the layers, these values correlate satisfactorily with the force constants calculated from experimental data. We also suggest that a more strongly bound material could be synthesized if either PbO structure has electrons removed from it.

Lead monoxide exists as two polymorphic forms: a tetragonal phase of red color, α-PbO, known under the name of litharge, and a yellow orthorhombic phase, β-PbO, known as massicot.[1] Both phases have very low electrical conductivity (≈10^{-12} mho/cm) but exhibit interesting semiconducting and photoconducting properties. For that reason, lead monoxide possesses potential applications of industrial importance in imaging devices, electrophotography, electroradiography, and laser technology. Other well-known fields of application of lead oxides are electrochemical batteries, paints, and silicate glasses. Recent investigations are reported of the diffusion coefficients,[2] dielectric constants,[3] thermal sensitization

[†]Permanent address: Laboratoire de Physique Quantique (CNRS, ERA 821), Université Paul-Sabatier, 31062 Toulouse, France.

(1) For preparations and chemical properties of PbO, see: (a) "Nouveau Traite de Chimie Minerale"; Pascal, P., Ed.; Masson: Paris, 1966; Vol. III, p 577. (b) Rochow, E. G.; Abel, E. W. "The Chemistry of Germanium, Tin, and Lead"; Pergamon Press: Oxford, 1973; p 119.
(2) Maier, J.; Schwitzgebel, G. *Mater. Res. Bull.* **1983**, *18*, 601.

0022-3654/84/2088-6696$01.50/0

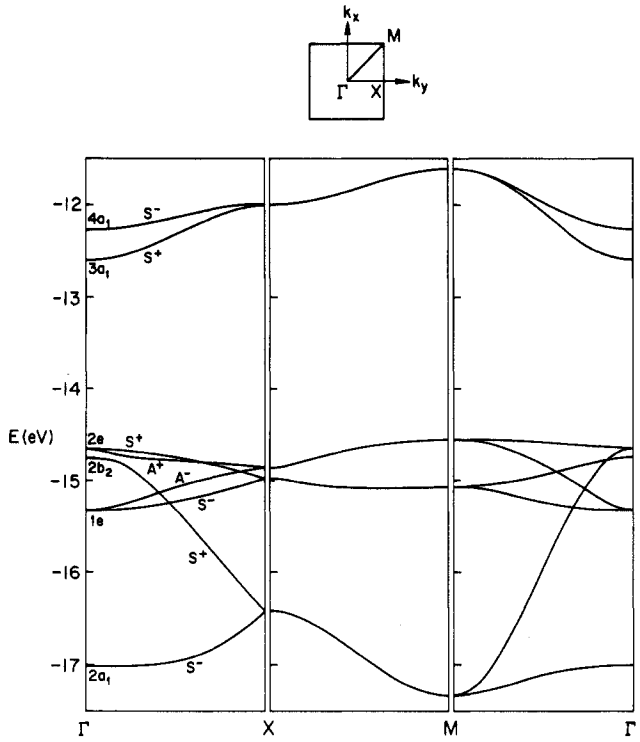

Figure 1. Occupied bands of a layer of α-PbO (the two inner bands, at −33 eV, are not shown).

of photoconductivity,[4] as well as phase transformations[5] or nonstoichiometric properties[6] of this material.

The structures of the lead monoxides α-PbO and β-PbO are well-knwon.[7-10] Both varieties are layer compounds, with characteristic easy cleavage and lubricant properties. The $\alpha \rightarrow \beta$ transformation occurs at 489 °C under atmospheric pressure. Although α is the low-temperature phase, β can be obtained below the transition temperature and simple mechanical treatment can induce the $\beta \rightarrow \alpha$ transition.

A layer of tetragonal α-PbO consists of a planar square grid of oxygen atoms (d_{O-O} = 2.80 Å) with lead atoms located alternatively on both sides of this mesh, as shown in **1a**. Each lead atom occupies the apex of a square pyramid formed by four equal Pb–O bonds (d_{Pb-O} = 2.30 Å). Each oxygen atom occupies the center of an imperfect tetrahedron formed by four equal Pb–O bonds. The layers are simply stacked (**1b**) so that each lead encounters four equal interlayer Pb–Pb contacts of 3.87 Å. It is commonly said that the apex of each square pyramid is actually occupied by the lead lone pair and that the layers are held together by van der Waals interactions between these lone pairs.

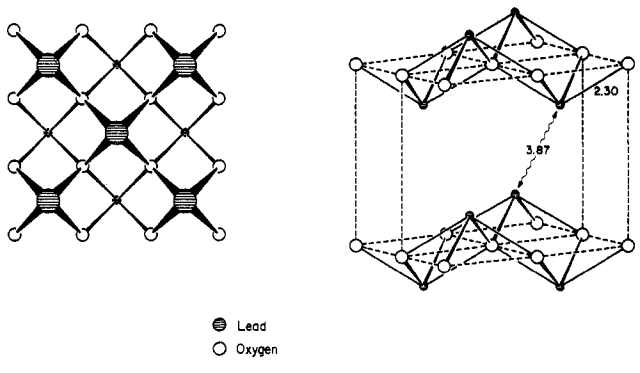

1

A layer of orthorhombic β-PbO is made up of parallel infinite –Pb–O–Pb–O– zigzag chains (see **2**). The intrachain PbO bond lengths are nearly the same, 2.21 and 2.22 Å, which is ≈0.1 Å shorter than in α-PbO. The chains are held together by interchain Pb–O bonds (2.49 Å).

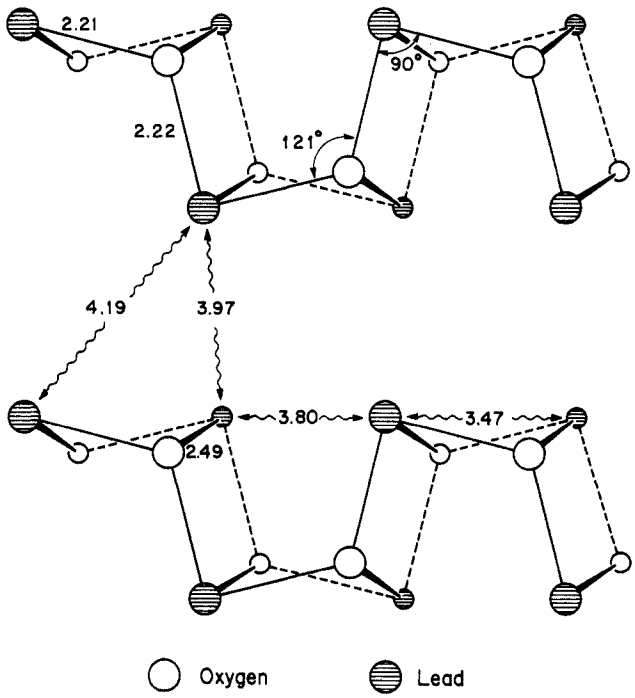

2

The link between the β-PbO and the α-PbO structures is shown in **3**. In β-PbO each lead atom occupies the apex of a distorted tetragonal pyramid, which is built with three different types of Pb–O bonds (2.21, 2.22, and 2.49 Å). Each oxygen atom occupies the center of a distorted tetrahedron constructed with the same three different types of Pb–O bonds. In short, a layer of β-PbO is a highly distorted layer of α-PbO. There are two kinds of interlayer Pb–Pb contacts (see **2**) which are both longer than in α-PbO (Pb_1–Pb_2 = 3.97 Å; Pb_1–Pb_3 = 4.19 Å). Again, as in α-PbO, since the interlayer Pb–O distances are large (3.81 Å for the shorter one), the layers are thought to be held together through van der Waals interactions between the lead lone pairs. Note that if we draw lone pairs (e.g., sp hybrids) on the lead atoms, these are not parallel to the stacking direction (c axis) in β-PbO whereas they are in α-PbO. Thus, Andersson et al.[11,12] have shown that

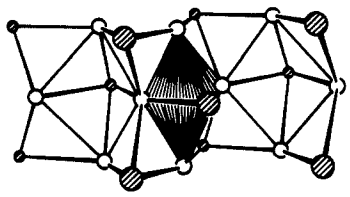

3

(3) Unoki, H.; Oka, K.; Nakamura, A. *Jpn. J. Appl. Phys.* **1981**, *20*, 2329.
(4) Radhakrishnan, S.; Kamalasanan, M. N.; Mehendru, P. C. *J. Mater. Sci.* **1983**, *18*, 1912.
(5) Okuri, Y.; Ogo, Y. *Bull. Chem. Soc. Jpn.* **1982**, *55*, 3641.
(6) (a) Kharif, Ya. L.; Sin'kowskii, S. I.; Datsenko, A. M.; Avetisov, I. Kh.; Kovtunenko, P. V. *Izv. Akad. Nauk SSSR, Neorg. Mater.* **1982**, *18*, 82. (b) Aurivillius, B. *Chem. Scr.* **1982**, *19*, 97. (c) For catalytic properties, see: Pacey, P. D.; Wimalasena, J. H. *Can. J. Chem.* **1983**, *61*, 1086.
(7) Leciejewicz, J. *Acta Crystallogr.* **1961**, *14*, 1304.
(8) Kay, M. I. *Acta Crystallogr.* **1961**, *14*, 80.
(9) Leciejewicz, J. *Acta Crystallogr.* **1961**, *14*, 66.
(10) Wells, A. F. "Structural Inorganic Chemistry", 4th ed.; Clarendon Press: Oxford, 1975; pp 100, 137, 218, 461, and 936.

in β-PbO the lead lone pairs (which are loated in the interlayer space) form with the oxygen atoms a regular hexagonal close-packed network. While the structure of β-PbO is unique, the structure of α-PbO is found for some other systems, such as valence isoelectronic SnO and LiOH (in this case the Li atoms form the square mesh).[10]

In **4** and **5** are schematized, for both phases of PbO, the pro-

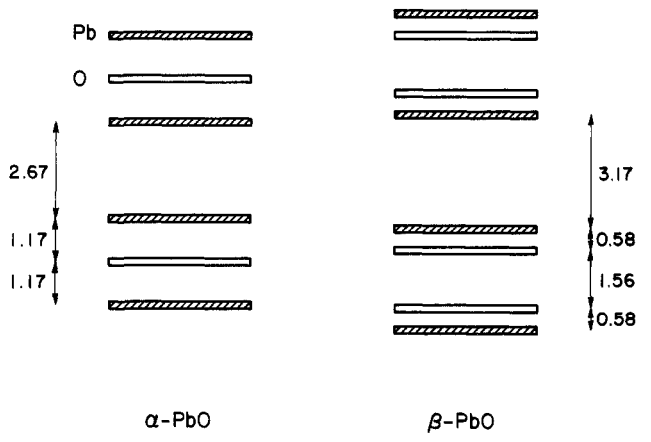

4 **5**

jections of the lead and oxygen sublayers forming the structure. This drawing makes clear that (1) lead is on the outside of the layers, and (2) in α-PbO the repeating slab comprises an oxygen sublayer sandwiched between two lead sublayers, whereas in β-PbO two oxygen sublayers are sandwiched between two lead sublayers.

In both lead monoxides, lead has formally an oxidation state II. Is there covalent bonding for each Pb–O link or do we have an ionic crystal with Pb^{2+} and O^{2-} ions? First, the structures of both solids show adjacent lead sublayers (see **4** and **5**) and this is not an optimal arrangement for strong ionic forces. Then, as Dickens has pointed out for β-PbO, there is very low symmetry in the immediate arrangement around both oxygen and lead and this too does not favor ionic forces in the crystal.

The first study of bonding in the lead monoxides is due to Dickens.[13] For yellow β-PbO and red α-PbO, Dickens built the relevant hybrids that account for the geometries. Burdett has studied the electronic structure of red α-PbO with molecular orbital (MO) techniques.[14] The structure of α-PbO is seen as a simple deformation from a CsCl type structure. This deformation is made necessry by simple electron-count arguments. Bordovskii et al. have published band structures of α-PbO[15] and β-PbO,[16] calculated with a semiempirical SCF method based on the Mulliken–Ruedenberg approximations. These authors are mainly interested in the electronic gaps rather than in the bonding in the solid. An interesting insight into the bonding in PbO, either within or between layers, is provided by the normal-coordinate analysis performed by Vigouroux, Calvarin, and Husson[17] on the Raman and IR vibrational spectra[18] of α- and β-PbO. The calculated force field is also discussed in relation with the abnormally small value of the thermal expansion along the direction normal to the layers.[19]

In the present work we examine the electronic structure and bonding in α- and β-PbO using quantum-mechanical calculations of the band structures of these two phases. We utilize extended Hückel[20] calculations, taking into account the lattice periodicity through the tight binding scheme.[21] Throughout this work we shall analyze the band structures focusing on the occupied (i.e., the valence) bands, which are responsible for the bonding in the solid. We are aware of the intrinsic limitations of our procedure, which ignores bielectronic coupling and correlation effects. Within the constraints of our approximate model we should not be able to see the van der Waals interactions which are supposed to be the only interlayer bonding forces.

α-PbO and β-PbO will be considered successively. For each phase, the layer first, and then the three-dimensional solid, will be studied. In the discussion we shall relate among other things our results to the known force constants. We shall also test the consequences of changing atomic parameters. The extended Hückel parameters, the geometries, and the special k point sets that we used are all listed in Appendix 1. In Appendix 2 we probe the consequences of changing atomic parameters for lead.

Tetragonal Red α-PbO

The unit cell chosen by us for the two-dimensional layer is shown in **6**. It consists of two PbO subunits forming a zenge

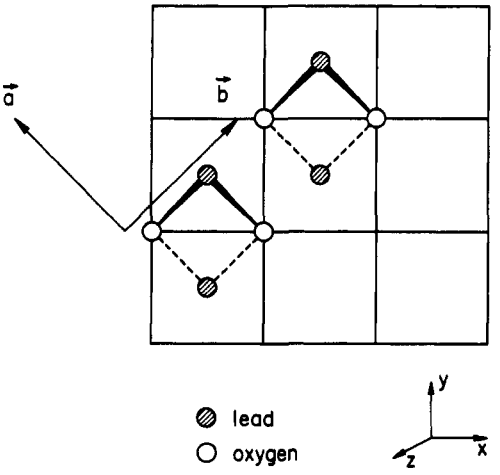

6

which is bent, with respect to the plane of the mesh of oxygens, one lead atom being up above and the other down below this plane.

The full set of calculated bands shows a very large gap between occupied and empty bands (≈8 eV), the Fermi level being at −11.62 eV. Given our basis set and unit cell, there are 16 bands, 10 which are occupied. In Figure 1 the bands are plotted (except for the two inner bands, which are located around −33 eV) along the three lines joining the symmetry points Γ, X, and M of the first Brillouin zone. At the zone center Γ, the crystal orbitals are classified within the C_{4v} point group, which is the symmetry of the whole crystal. The ΓX ($\vec{k}_y$) direction, which in our square system is the same direction as the direct lattice vectors $\vec{a}$ and

(11) Andersson, S.; Åström, A. *NBS Spec. Publ.* **1972**, *No. 364*, 3.
(12) Galy, J.; Meunier, G.; Andersson, S.; Åström, A. *J. Solid State Chem.* **1975**, *13*, 142.
(13) (a) Dickens, B. *J. Inorg. Nucl. Chem.* **1965**, *27*, 1495. (b) Dickens, B. *J. Inorg. Nucl. Chem.* **1965**, *27*, 1503.
(14) Burdett, J. K.; Lin, J.-H. *Acta Crystallogr. Sect. B* **1981**, *B37*, 2123. Burdett, J. K. *Adv. Chem. Phys.* **1982**, *49*, 47.
(15) Bordovskii, G. A.; Gordeev, N. L.; Ermoshkin, A. N.; Izvozchikov, V. A.; Evarestov, R. A. *Phys. Status Solidi B* **1983**, *115*, K15.
(16) Bordovskii, G. A.; Gordeev, N. L.; Ermoshkin, A. N.; Izvozchikov, V. A.; Evarestov, R. A. *Phys. Status Solidi B* **1983**, *111*, K123.
(17) Vigouroux, J. P.; Calvarin, G.; Husson, E. *J. Solid State Chem.* **1982**, *45*, 343.
(18) (a) Donaldson, J. D.; Donaghue, M. T.; Ross, S. D. *Spectrochim. Acta, Part A* **1974**, *30A*, 1967. (b) Adams, D. M.; Stevens, D. C. *J. Chem. Soc., Dalton Trans.* **1977**, *1096*.
(19) (a) Garnier, P.; Calvarin, G.; Weigel, D. *J. Chim. Phys.* **1972**, *11-12*, 1711. (b) Sorrell, C. A. *J. Am. Ceram. Soc.* **1970**, *53*, 552. (c) Sorrell, C. A. *J. Am. Ceram. Soc.* **1970**, *53*, 641.
(20) Hoffmann, R. *J. Chem. Phys.* **1963**, *39*, 1397.
(21) (a) Whangbo, M.-H.; Hoffmann, R. *J. Am. Chem. Soc.* **1978**, *100*, 6093. (b) For the first extensive application of this method to the band structures of polymers, see: Whangbo, M.-H.; Hoffmann, R.; Woodward, R. B. *Proc. R. Soc. London, Ser. A* **1979**, *366*, 23. (c) Methodological details can be found in: Hughbanks, T.; Hoffmann, R. *J. Am. Chem. Soc.* **1983**, *105*, 1150.

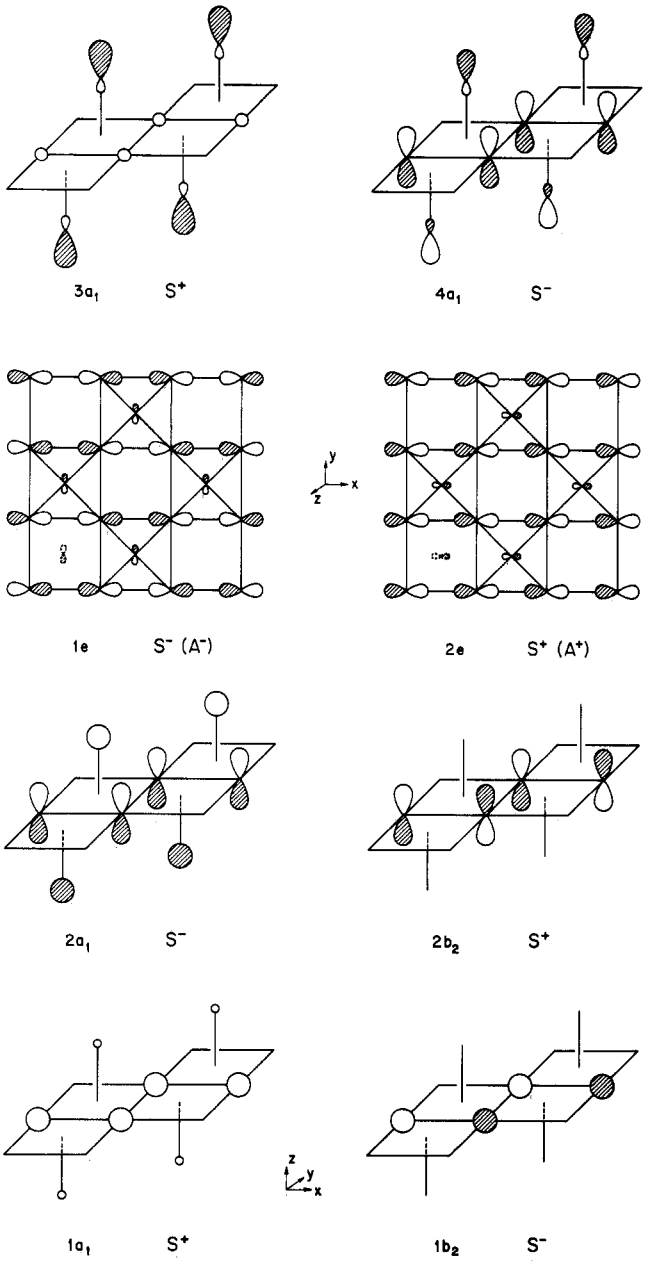

Figure 2. Crystal orbitals at the Γ point for two-dimensional α-PbO.

$\vec{b}$, is nonsymmorphic. There is a screw axis Λ along this line. The other element of symmetry on this line is a vertical plane of symmetry. Thus, the orbitals may be classified along this line as S or A (plane of symmetry) indexed with + or − (screw axis). Along the XM line, all orbitals are doubly degenerate and are of the same symmetry. In M the degeneracy is broken, and from M to Γ the element of symmetry is a C_2 axis. All occupied orbitals at the zone center Γ are drawn in Figure 2. Let us discuss them at Γ point and along the ΓX direction.

First, we find two inner bands, around −33 eV, corresponding to the bonding $1a_1$ and antibonding $1b_2$ combinations of the oxygen 2s orbitals (Figure 2, bottom). Along the ΓX line, $1a_1$ is destabilized and $1b_2$ stabilized until, at the zone edge, both orbitals are degenerate. Then we find a $2a_1$ orbital which is the real Pb–O bonding orbital, involving a bonding combination of the oxygen 2p orbitals with the lead 6s orbitals. This orbital is destabilized along the ΓX line, as can be expected from the phases of the atomic orbitals involved. One can see in Figure 2 that this orbital has C_s symmetry and is antisymmetric with respect to the screw axis. More than 2 eV above (at the Γ point), the $2b_2$ orbital corresponds to the out-of-phase combination of the oxygen p_z orbitals. This time no orbital from lead has the right symmetry to contribute. Actually, d_{xy} orbitals would have the right symmetry, **7**, and inclusion of d orbitals in the basis set of lead (which

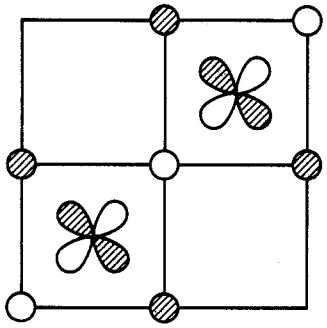

7

we did not do) could have stabilized this $2b_2$ orbital. Along the ΓX line, this orbital is stabilized; and at the zone edge it is degenerate with $2a_1$. Note in Figure 4 the large dispersion of this band along the ΓX direction.

We encounter then two sets of e orbitals. The first set, labeled 1e, is the σ-bonding and π-antibonding combination of the p_x (or p_y) orbitals of oxygen. This configuration allows the lead p_y (or p_x) orbitals to be involved to a small extent in a bonding way (see Figure 2). Within this 1e set, one can do an appropriate mixing to obtain symmetrical and antisymmetrical combinations with respect to the symmetry plane. Along the ΓX line, these e orbitals become S^- and A^-. The second set, 2e, higher in energy, is the σ-antibonding + π-bonding combination of the p_x (or p_y) orbitals of oxygen (see Figure 2). This 2e set gives S^+ and A^+ orbitals along the ΓX line. There is no surprise that this e set is higher in energy than the previous one, because, if we keep in mind that the oxygen atoms are spaced 2.30 Å apart, the π overlap is very weak. However, the nodal properties do not favor particularly the 1e set over the 2e set, as can be seen from the projections of the nodal surfaces, **8**, **9**.

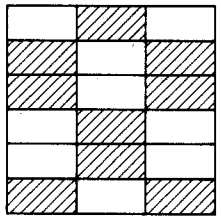

8, 1e

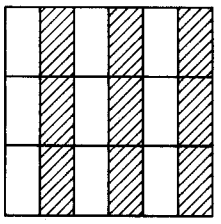

9, 2e

Along the ΓX line, the orbitals from the 1e set lose their properties of "all σ-bonding". At the zone edge, the combination of the oxygen p_x orbitals becomes schematically half σ-bonding, half π-bonding (**10**), and the corresponding orbitals are destabilized

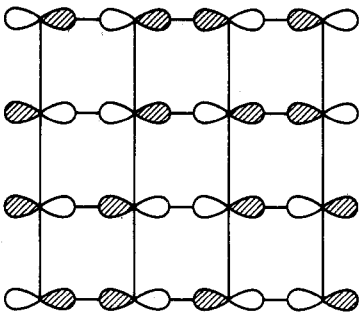

10

(Figure 1). Another way of representing this is to recognize only the two kinds of bonding connections in the mesh of oxygens, **11**,

12. Similarly, along the ΓX line, the orbitals from the 2e set

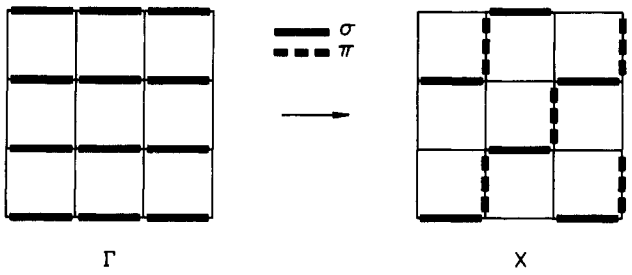

11 **12**

which were all π-bonding become at the zone edge half σ-bonding, half π-bonding (**13**, **14**) and are therefore stabilized. Equivalency

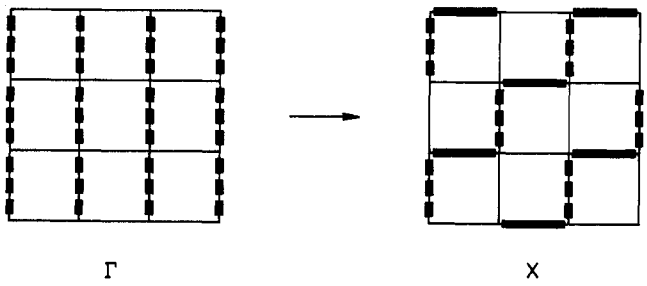

13 **14**

of **12** and **14** implies that orbitals from the 1e and 2e set will be degenerate at the zone edge. This is what happens (see Figure 1) although things are made a little more complicated by the mixing and our reasoning is intentionally simplified. Note that at X point the degeneracies occur between S^- and S^+ and A^- and A^+. Note also that on the whole the dispersion of these bands is weak because the σ and π overlap between the p orbitals of the 2.30 Å distant oxygens is weak.

The last two orbitals, $3a_1$ and $4a_1$ at the Γ point, are important since they correspond to the lone pairs of lead and therefore will be involved in the interlayer bonding. They are constructed from the in-phase ($3a_1$) and out-of-phase ($4a_1$) combinations of the lead sp hybrids which point away from the layer. In $3a_1$, a small admixture of the oxygen s orbital is found. In $4a_1$, the oxygen p_z orbitals have a large contribution. From the phases of the atomic orbitals, one can infer that both crystal orbitals will be destabilized along the ΓX line. This is what happens in Figure 1. At the zone edge, the two orbitals are degenerate.

We shall not comment on the band structure for the other directions. The dispersions along the ΓM line have some similarity with the ones along the ΓX line. Within the two-dimensional layer, the resulting overlap population between Pb and O is 0.119. Between "up and down" leads (inside the unit cell), the overlap population is −0.011; between leads from the same side of the layer, it is 0.000; and between the oxygens, it is calculated at −0.003.

When the layers are stacked together, the bands that will be perturbed will be the ones that have lobes pointing away from the layer in the *z* direction. These are $2a_1$ and mainly $3a_1$ and $4a_1$. From the phase of the lobes pointing up and down the mesh of oxygens, one can predict the evolution of these orbitals at the Γ point as one moves from the two-dimensional layer to the three-dimensional solid. We shall discuss also the evolution along the lines ΓX and ΓZ (the direction of the stacking) for the three-dimensional solid.

The bands for the three-dimensional solid of stacked layers are plotted along the main line of the first Brillouin zone in Figure 3. Let us discuss what happens at the Γ point, from the two-dimensional layer (Figure 1) to the three-dimensional solid (Figure 3). To this end we shall use the projection of the lead orbitals of two layers onto a horizontal plane located midway between these

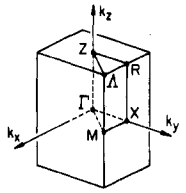

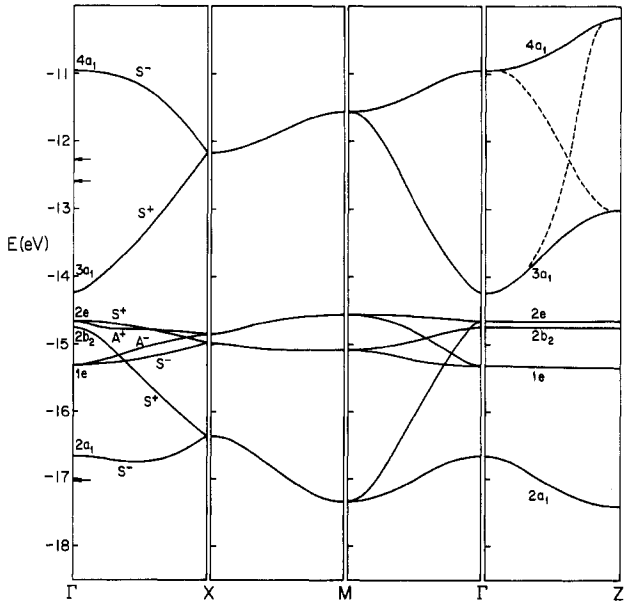

Figure 3. Occupied bands of three-dimensional α-PbO (the two inner bands, at −33 eV, are not shown). The arrows indicate the position of $2a_1$, $3a_1$, and $4a_1$ at the Γ point in the two-dimensional layer.

two layers. It becomes clear that $3a_1$ should be stabilized by the stacking (**15**), whereas $4a_1$ should be destabilized by the stacking

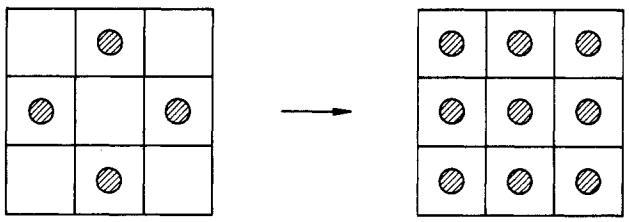

15

(**16**). $2a_1$ is also destabilized by the stacking, though to a lesser

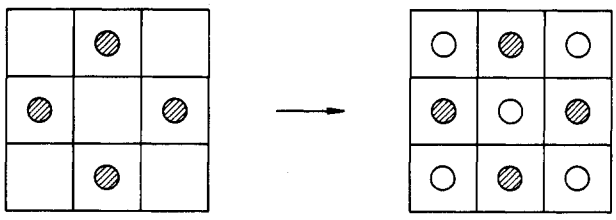

16

extent. All this actually occurs at the Γ point, as may be seen from Figures 1 and 3. Along the ΓX line, $3a_1$ is destabilized (**17**), and $4a_1$ is stabilized (**18**), both being degenerate at X point.

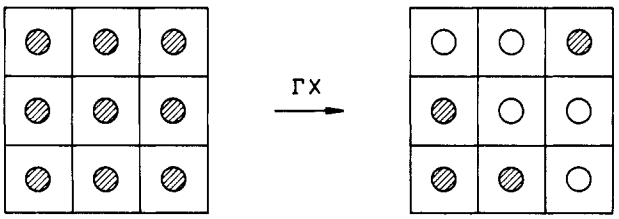

17

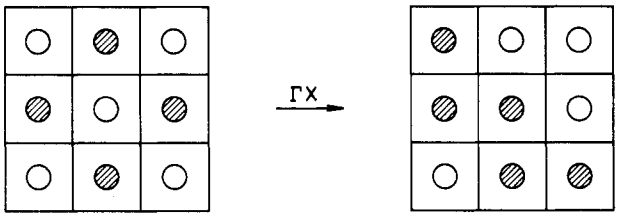

18

An important point is that $4a_1$ is destabilized less at Γ and elsewhere in the Brillouin zone than $3a_1$ is stabilized. This is the reverse of what is usually observed in pairwise orbital interaction: normally the overlap term makes an antibonding orbital go up from some nonbonding reference state more than the bonding combination goes down. If both orbitals are occupied, the net result is a four-electron destabilization.

Since this expected effect of direct Pb–Pb interlayer interaction is not what happens, it must be that some unfilled orbitals of each layer mix into $3a_1$ and $4a_1$ as the layers stack, stabilizing both. The orbitals that mix in are higher bands, corresponding to Pb–O σ^* levels. The four-electron repulsive interlayer interaction is thus alleviated by a two-electron attractive interaction—there is some real bonding between the layers. We will return to this point again.

The ΓZ line, which corresponds to the direction of the stacking, is symmorphic. The symmetry along this line is the symmetry of the solid, namely C_{4v}. In Figure 3 one can see that along this line only our three orbitals $2a_1$, $3a_1$, and $4a_1$ are dispersed. $3a_1$ should be destabilized (**19** → **20**), and $4a_1$ (as $2a_1$ to a lesser extent)

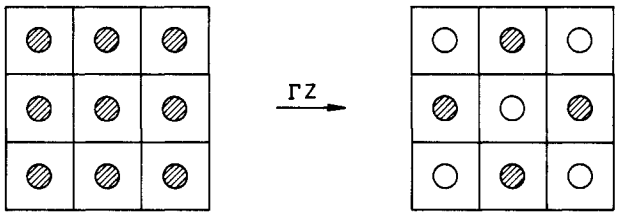

19 20

should be stabilized (**21** → **22**). According to this simple scheme

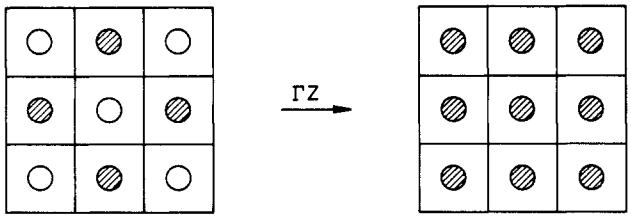

21 22

a crossing of these two orbitals can be expected. Since they are both of the same symmetry, a_1, along this line, these two orbitals will avoid the crossing. This is what happens. Along the ΓZ line,

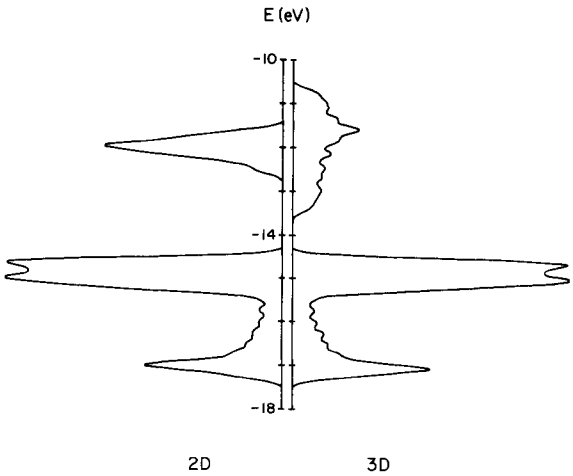

Figure 4. Density of states in one layer of α-PbO (left) and in the three-dimensional solid (right).

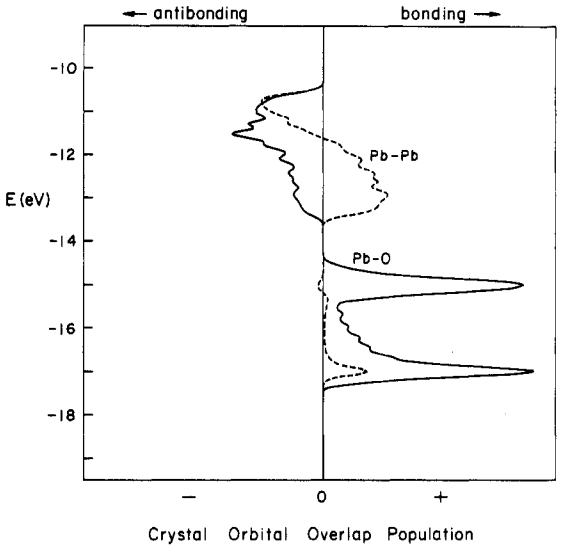

Figure 5. Crystal orbital overlap populations (COOP) curves for intralayer Pb–O (—) and interlayer Pb–Pb (- - -) in three-dimensional α-PbO.

there is strong mixing and inspection of the crystal orbitals at the Γ point and at the Z point clearly shows that $3a_1$ and $4a_1$ have inverted their nature. The fact that $3a_1$ is more dispersed than $4a_1$ along ΓX and ΓZ (if one remembers the crossing) may come from the nature of $3a_1$, involving mainly lead hybrids, whereas $4a_1$ involves half lead hybrids and half oxygen p_z atomic orbitals.

The main effect of the stacking is therefore a broadening of the highest occupied bands. This also can be seen in the curves of the density of states (DOS) displayed in Figure 4. The Fermi level for the three-dimensional solid is now at −10.15 eV and the electronic gap has been reduced to 4.96 eV. The resulting overlap populations are +0.116 for intralayer Pb–O and +0.030 for interlayer Pb–Pb. We obtain a net charge of +1.57 on each lead atom. For this experimental geometry, the overlap population index therefore indicates a certain degree of bonding between lead atoms belonging to different layers. The corresponding interlayer Pb–Pb distance is large (3.87 Å) but this is only 0.4 Å larger than the interatomic distance in metallic lead. Small positive overlap populations, in our experience, are often reliable indicators of incipient bonding interactions. We proceed to examine these stacking interactions in greater detail.

In Figure 5 are shown the crystal orbital overlap population (COOP) curves[22] for the bonds Pb–O intralayer and Pb–Pb in-

(22) For other examples of the use of COOP curves, see: (a) Hughbanks, T.; Hoffmann, R. *J. Am. Chem. Soc.* **1983**, *105*, 3528. (b) Kertesz, M.; Hoffmann, R. *J. Am. Chem. Soc.* **1984**, *106*, 3453. (c) Saillard, J.-Y.; Hoffmann, R. *J. Am. Chem. Soc.* **1984**, *106*, 2006.

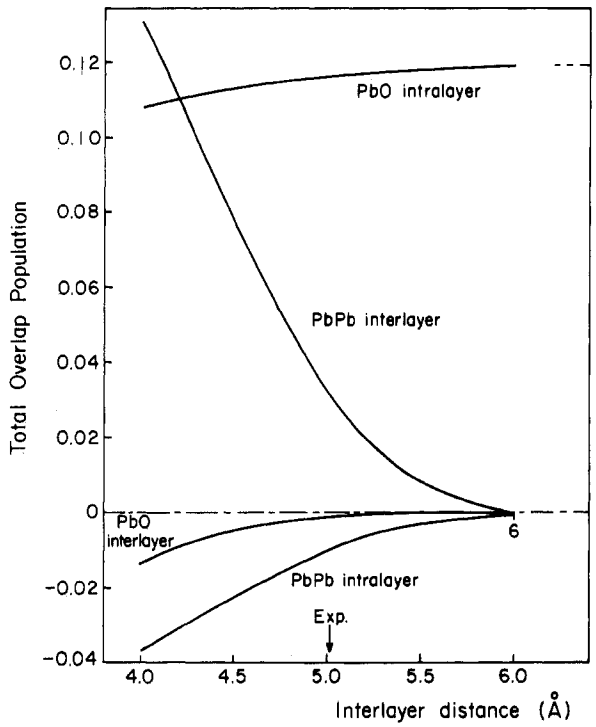

Figure 6. Evolution of some overlap populations, as a function of the stacking of the layers of α-PbO. The interlayer distance is the vector **c** of the direct lattice.

terlayer. These curves represent the density of states weighted by the overlap populations. Around a given energy the electronic states contribute to bonding or antibonding between the two given atoms according to whether the curve is in the positive (right) or negative (left) part of the diagram, respectively.

One can see in Figure 5 that the ends of the set of bands $2a_1$, $2b_2$; 1e and 2e at the Γ point (−17 to −15 eV) contribute to the Pb–O bonding while the two highest bands ($3a_1$ and $4a_1$ at Γ point) have an antibonding contribution to the Pb–O bond. The bands which contribute to the interlayer Pb–Pb bonding are the bottom of the $2a_1$ band around −17 eV and the bottom of the set $3a_1$, $4a_1$. The top of this set, i.e., the top of the occupied bands, is antibonding for both interlayer lead–lead and intralayer lead–oxygen. An intriguing consequence of this is that were we to drain a certain number of electrons from the solid, the total overlap population for these two bonds should increase. A decrease of the corresponding bond lengths should ensue, giving a stronger cohesion within the layers and between layers. This could be accomplished by acceptor species, interstitial or not, or by any oxidative procedure.

In order to shed more light on the bonding in the solid, and especially that between layers, let us see what happens when layers are progressively brought together from an infinite separation. The variations of the overlap populations during this stacking are shown in Figure 6. The largest variation corresponds to the interlayer Pb–Pb bond. This overlap population strongly increases when the layers are stacked beyond the experimental interlayer distance, i.e., corresponding to Pb–Pb distances less than 4 Å. However, for the experimental interlayer distance, corresponding to a distance Pb–Pb = 3.87 Å, the overlap population is still weak (+0.030). One can also notice that during the stacking (1) the intralayer Pb–O overlap population decreases slightly, (2) intralayer Pb–Pb becomes negative, but is still weak at the experimental geometry (−0.010), and (3) interlayer Pb–O becomes negative but is still near zero at the experimental geometry, the corresponding Pb–O bond length still being large (4.32 Å).

The energy variation during the stacking is drawn in Figure 7. The curve is repulsive, with a local minimum at a 4.3-Å interlayer distance. This corresponds to a Pb–Pb interlayer distance of 3.4 Å, which, incidentally, is close to the interatomic distance in metallic lead (3.5 Å). The origin of this singularity

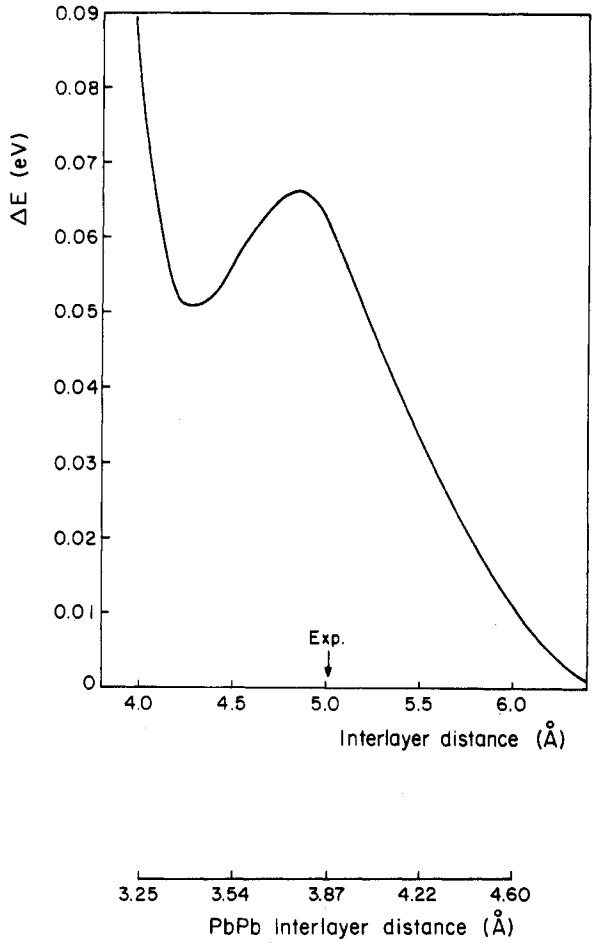

Figure 7. Relative variation of the total energy per PbO unit as a function of the stacking of the layers of α-PbO.

in energy variation could be some level crossing. However, we were unable to identify it clearly from the wave functions. It is probably some avoided crossing between occupied and empty bands. The same COOP curves as those plotted in Figure 5 have been plotted for an interlayer distance close to the local energy minimum. They are pretty similar to Figure 5 up to ≈−12 eV. In the upper part, both curves are spread out and the Pb–Pb curve is now hardly antibonding.

There is another indicator of direct interlayer bonding in Figure 5. If the interaction between layers were based only on Pb–Pb interactions, the top bands in the material should be Pb–Pb bonding at the bottom of the band, and Pb–Pb antibonding at the top of the band. But, as we mentioned above, the inclusion of the overlaps would make the bonding weaker in its part of the band, compared to the antibonding in the upper part of the band. The overlap populations should reflect this, and do so in model calculations. But in PbO, as the COOP curves of Figure 5 show, the top of the valence band is less Pb–Pb antibonding than the bottom of that band is bonding. This can only happen through stabilizing mixing between this valence band and conduction bands which are Pb–O σ^* in character.

Orthorhombic Yellow β-PbO

The planar zigzag chains in β-PbO suggest a logical building up of the three-dimensional structure, which we will follow. We shall start from the simplest entities, the atoms, and we shall build successively the diatom, the chain, the layer, and the three-dimensional solid. An important step in this analysis will be the passage from the diatom, which is the real subunit, to the chain, using a screw axis.

Appendix 2 will be devoted to a comparison of the results obtained from two different sets of lead parameters. The present section is based on calculations made by using a set of parameters that we call "relativistic". The same parameters were also used

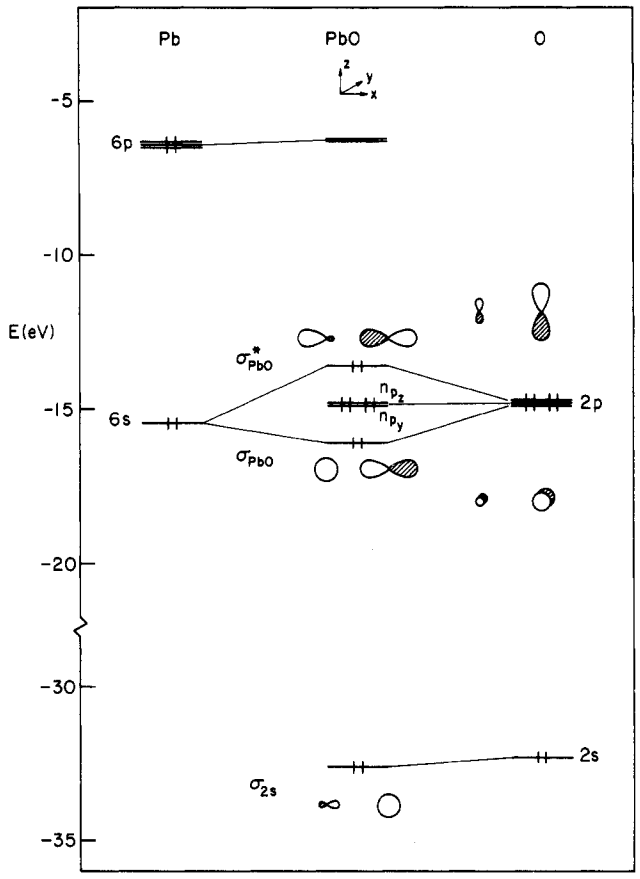

Figure 8. Schematic interaction diagram for diatomic PbO.

for α-PbO. With this set of parameters, there is a good energy matching between the orbitals 6s of lead and 2p of oxygen. This results in the formation of σ and σ^* bonds when the diatom is built from the two atoms. A simplified interaction diagram for PbO is shown in Figure 8. The inner orbital is made up essentially from the oxygen 2s orbital with a very small amount of lead 6p orbital. Then we have the σ-bonding and σ^*-antibonding combinations of $2p_x$ (O) with 6s (Pb). Note that the two atoms contribute equally to these two orbitals, the reduced charge matrix giving 1.0 on each atom in both orbitals. Between them there are the degenerate orbitals corresponding to the 2p oxygen lone pairs, with a tiny admixture of lead 6p orbitals.

Given the diatom MO's, one can now construct the crystal orbitals of the one-dimensional zigzag chain using the screw axis, **23**, and the overlap and energy matching. The unit cell consists

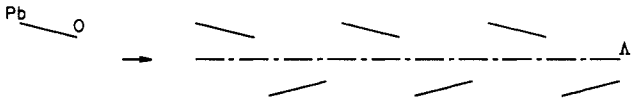

23

of two PbO subunits. The two elements of symmetry at the zone center and throughout the one-dimensional Brillouin zone are a plane of symmetry (the plane of the chain) and a screw axis (the direction of the chain). The crystal orbitals will be classified therefore as S or A (or a′ or a″), indexed with + or −.

The occupied bands of the chain are plotted in Figure 9. The shapes of the orbitals at the zone center are drawn in Figure 10 for two unit cells. Let us comment on these orbitals at the Γ point.

The first set of orbitals, around −33 eV, is not plotted in Figure 9. It corresponds to the in-phase (1a′) and out-of-phase (2a′) combinations of the σ_{2s} orbitals mainly localized on oxygen. We then encounter the two combinations of σ_{PbO}, 3a′ (S^-) and 4a′ (S^+). Of course, on going from the diatoms to the chain the p orbitals mix (or rotate) to improve the overlap, as for instance in 3a′ (**24**). Above these bands we have four bands corresponding to the lone

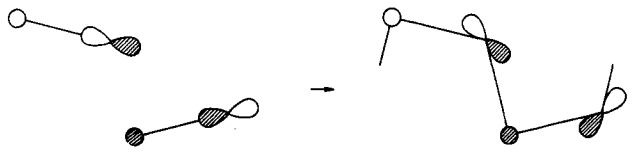

24

pairs of oxygen, which are therefore very little dispersed. These are 5a′ (S^+) and 6a′ (S^-), coming from oxygen np_z, and 1a″ (A^-) and 2a″ (A^+), coming from oxygen np_y. Note that the p orbitals of lead can participate in 5a′, 6a′, and 1a″ but not in 2a″. Here also, the use of d orbitals on lead could have changed this, since a mixing of d_{xy} and d_{yz} would have the right symmetry, **25**, to

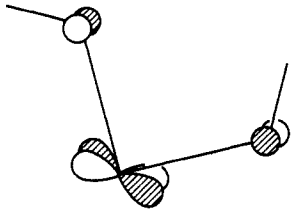

25

stabilize this orbital. Finally, about 2 eV above in energy, we find the two bands built from σ^*_{PbO}, 7a′ (S^+) and 8a′ (S^-). Actually, strong mixing occurs and 7a′ has larger coefficients on lead. These two highest occupied bands have lobes pointing away from the chain in the O_z direction. Therefore, they will be involved in the interlayer bonding. On the other hand, one can expect that the bands 1a″ and 2a″, which point in the O_y direction, will be involved in the interchain bonding.

The COOP curves corresponding to some bonds in the chain are displayed in Figure 11. Here also, the upper part of the occupied bands is antibonding for PbO. The total overlap populations are calculated to be 0.174 for PbO short, 0.171 for PbO long, +0.004 for 1,4-PbO, −0.011 for 1,3-PbPb, and −0.011 for 1,3-OO. The Fermi level if −12.61 eV, with a gap of 6.30 eV. The net charge on lead is calculated at +1.68.

The layer is built by stacking the planar chains parallel to each other. In fact, each zigzag chain is inverted and shifted in the x direction with respect to its neighboring chains so that the unit cell is now two $(PbO)_2$ subunits, although all lead atoms and all oxygen atoms are still equivalent. Because of this doubling of the unit cell, each band of the one-dimensional chain will be duplicated, resulting in 20 occupied bands. The 16 highest occupied bands of the layer, in its experimental geometry, are plotted in Figure 12. The bands pointing in the y direction, i.e., the a″ bands (A^+ and A^-) give a new set lower in energy. For the two other important sets (3a′ and 4a′, and 7a′ and 8a′) the duplication is made toward higher energy. A consequence of this is that the Fermi level is now at −11.60 eV but the gap is still 6.30 eV. Figure 13 displays the density of states for both the chain and the β-PbO slab. The crystal orbitals corresponding to the four upper bands are drawn in Figure 14. They will be involved in the interlayer bonding. To understand what links the chains together (i.e., the interchain or intralayer bonding) one can look at the total overlap population for the three main interchain bonds Pb–O, Pb_1–Pb_4, and Pb_1–Pb_5 (to keep the notations of ref 17), **26**. The calculated

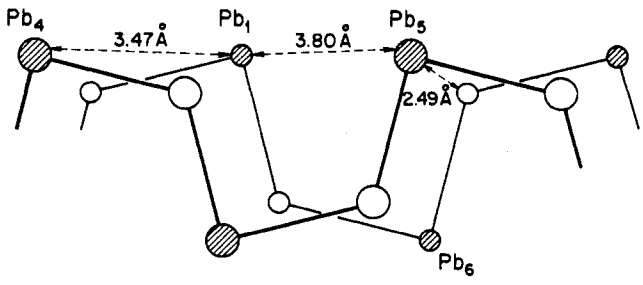

26

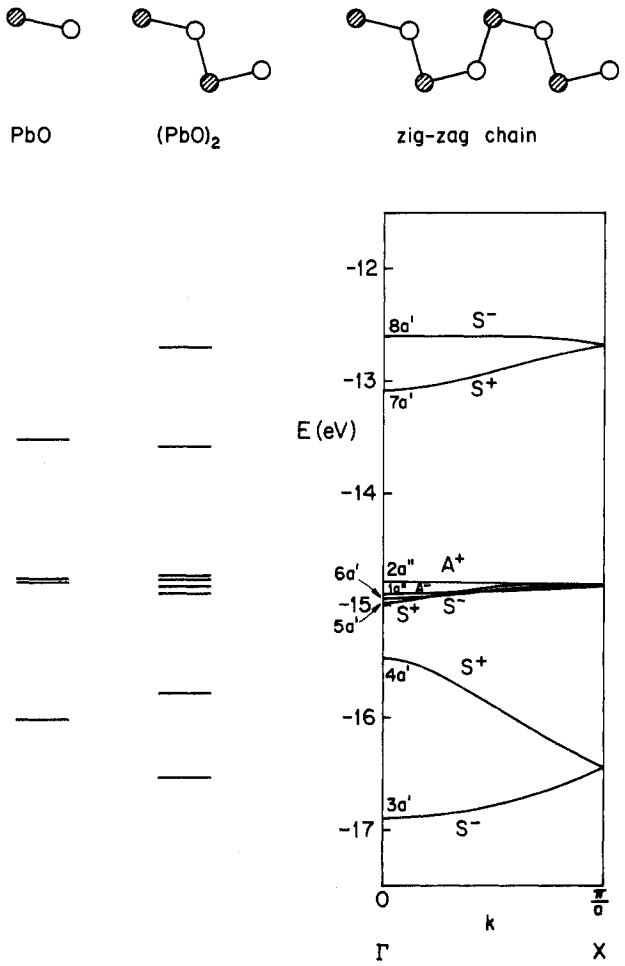

Figure 9. Occupied bands of the one-dimensional α-PbO chain. The two inner bands around −33 eV are not shown. The molecular orbital levels of the diatom PbO and the unit cell $(PbO)_2$ are shown for purposes of comparison.

overlap populations for these bonds are Pb–O = 0.066, Pb_1–Pb_4 = 0.022, and Pb_1–Pb_5 = 0.036. Note that the longer Pb–Pb bond has the larger overlap population; we shall come back to this result later in this work. Thus, the Pb–Pb bonds contribute significantly to the interchain linking. The corresponding COOP curves are plotted in Figure 15. The contribution of the bands to Pb–O bonding and antibonding is similar for intrachain Pb–O and interchain Pb–O (Figure 15, right), with the characteristic antibonding contribution at the top of the valence band. The main contribution to the interchain Pb–Pb bonding comes from the upper set of bands. Note in Figure 15 that the top of the valence band is bonding for Pb_1–Pb_4 and antibonding for Pb_1–Pb_5. This means that removal of electrons from this layer should reinforce Pb_1–Pb_5 and weaken Pb_1–Pb_4, as well as all Pb–O's. This should slightly decrease the intrachain Pb–O bonds and the interchain distance, but since Pb_1–Pb_5 should be shortened while Pb_1–Pb_4 should be lengthened, a resulting shearing of the chains, **27**, might also occur.

Let us now bring the chains together. The energy curve corresponding to this movement is plotted in Figure 16. This potential curve has a minimum around an interchain distance of 3 Å which corresponds to interchain distances PbO = 3.1 Å, Pb_1–Pb_4 = 3.9 Å, and Pb_1–Pb_5 = 4.2 Å. This potential well corresponds to 0.13 eV per PbO unit and shows that there are real bonds between chains. However, the position of the minimum does not correspond to the experimental interchain distance. At that distance, 2.39 Å, the system is at +0.34 eV with respect to an infinite interchain distance. This is not really a surprise since it is known that extended Hückel calculations generally do not give reliable potential surfaces as far as distances are concerned.

The variations of the total overlap populations during this

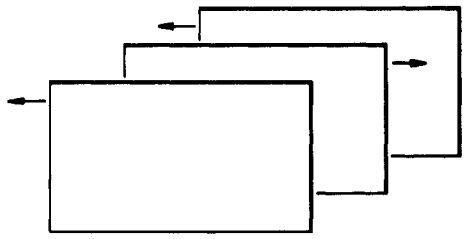

27

motion are given in Figure 17. Interchain PbO bonding increases strongly with a decrease of the interchain distance. Another effect of the stacking is the decrease of intrachain PbO overlap populations, and especially that of the horizontal (short) bond, which is smaller than that of the vertical (long) one at the experimental interchain distance. At that distance, one will note also that the Pb_5–Pb_6 overlap population (see **26**) has become negative.

Let us now summarize our results on the α-PbO and β-PbO layers or slabs. In both compounds, the main links in the layer are PbO bonds. In α-PbO, each oxygen atom is involved in four equal PbO bonds (2.30 Å) disposed tetrahedrally around that atom. We have calculated the overlap population for such bonds at 0.119. In β-PbO, each oxygen atom is involved also in four PbO bonds which are also disposed pseudotetrahedrally but which are not equivalent: two of them are intrachain bonds (short, 2.21 Å; long, 2.22 Å) and the other two are interchain bonds (2.49 Å). The corresponding overlap populations were calculated at 0.155, 0.164, and 0.066, respectively. The sum of the overlap populations around oxygen is therefore 0.476 for α-PbO and 0.451 for β-PbO. Now, neglecting all the O–O interactions, which are weak in both cases, let us do a similar count around the lead atom. In α-PbO, each lead is involved in four equivalent square-pyramidal PbO bonds; in β-PbO, each lead is also involved in four pseudo-square-pyramidal PbO bonds which are not equivalent. Up to now we have a similar count as for the oxygen centers, but a difference between the two layers occurs with the Pb–Pb bonds. In α-PbO, all intralayer Pb–Pb links are weak and the sum of the Pb–Pb overlap populations around each lead atom is (4)(0.000) + (4)(−0.011) = −0.044. In β-PbO we have relatively strong Pb–Pb links and the sum is (2)(0.036) + (2)(0.022) + (2)(−0.007) + (2)(−0.013) = 0.076. So, according to all these indexes, the layer of β-PbO would be more covalently bonded than the layer of α-PbO, and this because of the Pb–Pb bonds in β-PbO. In any case, for the experimental geometries, our calculations give the layer of β-PbO 0.43 eV lower in energy than the layer of the α-modification.

As for α-PbO, when the layers of β-PbO are stacked together to give the three-dimensional solid, the bands which will be perturbed will be the ones that point in the z direction. These are mainly the set of the four highest occupied bands 13a′–16a′ given in Figure 14. From the phases of the lobes pointing up and down in the z direction, one can predict, as in the case of α-PbO, on which side these orbitals will be shifted, at the Γ point, as we go from the two-dimensional layer to the three-dimensional solid. To this end, let us use the drawings of Figure 14 and a projection onto an interlayer plane, as we did for α-PbO. The mesh of projected lead atoms is not perfectly square since there are now two kinds of interlayer Pb–Pb bonds, Pb_1Pb_2 (3.97 Å) and Pb_1Pb_3 (4.19 Å), but in our drawings we shall simplify to square meshes.

At the Γ point the effect of the stacking on 13a′ should stabilize this orbital (**28**). The band structure of three-dimensional β-PbO along the five main directions of the first Brillouin zone is plotted in Figure 18. One can see at the Γ point that actually 13a′ (S^+) has been pushed down by nearly 1 eV. Similarly 14a′ is pushed up to about the same extent (**29**). Such effects are less obvious

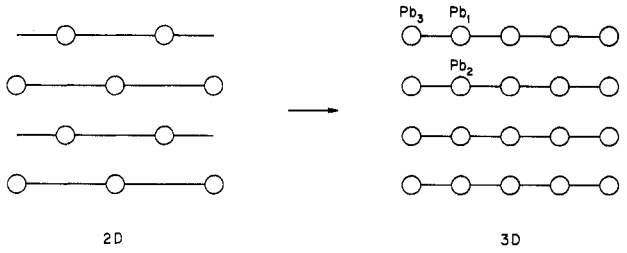

28

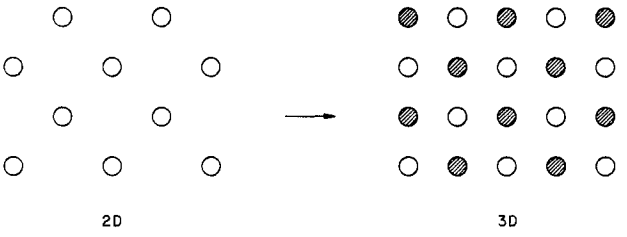

29

for 15a′ and 16a′. Only if we keep in mind that Pb_1Pb_2 (i.e., the vertical bonds in our schematic mesh) is shorter than Pb_1Pb_3 (i.e., the horizontal bonds), then it becomes clear that 15a′ (S^+) should be slightly destabilized (**30**) and 16a′ (S^-) should be slightly

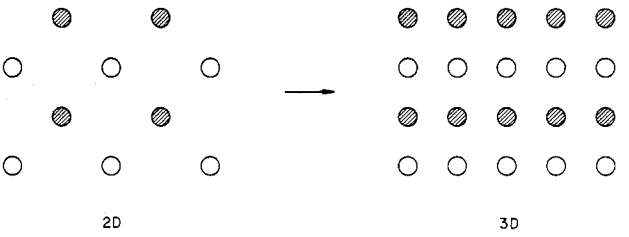

30

stabilized (**31**). Actually these two orbitals have been modified

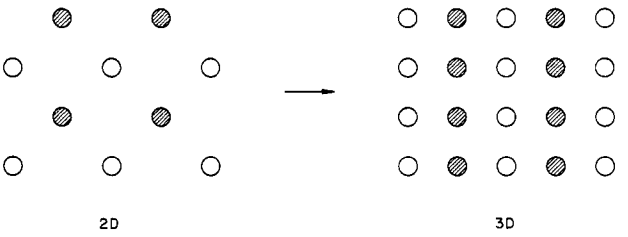

31

in this way at the Γ point and have crossed each other. One can see in Figure 18 that the two highest occupied orbitals at the Γ point are now S^+ above S^-.

Along the ΓX line, 13a′ (S^+) is destabilized (**32**) and 14a′ (S^-)

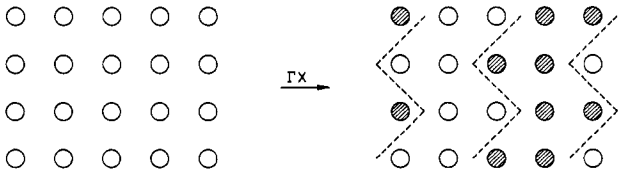

32

is stabilized (**33**), both being degenerate at the X point. According to such simple considerations, 15a′ (S^-) should be destabilized and 16a′ (S^+) stabilized along the ΓX line. In fact (see Figure

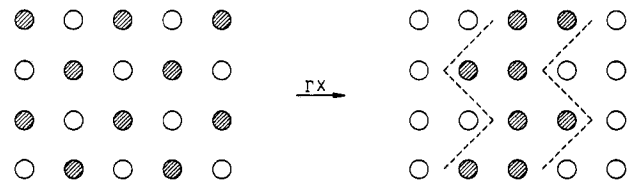

33

18), both are slightly destabilized but, as expected, the dispersion is very weak for these two bands along the ΓX direction.

Along the ΓZ direction, 13a′ is pushed up (**34**) and 14a′ is pushed down (**35**). As in the case of α-PbO, this gives rise to an avoided band crossing (see Figure 18).

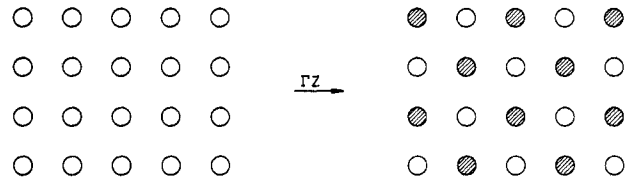

34

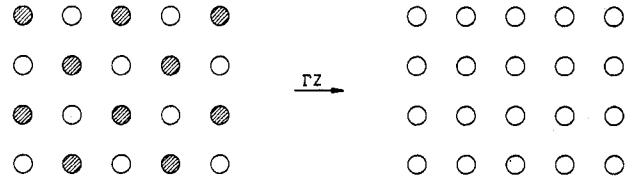

35

Again if we take into account that $Pb_1Pb_2 < Pb_1Pb_3$, 15a′ should be destabilized (**36**) and 16a′ should be stabilized (**37**). This gives also an avoided band crossing which has been indicated in Figure 18.

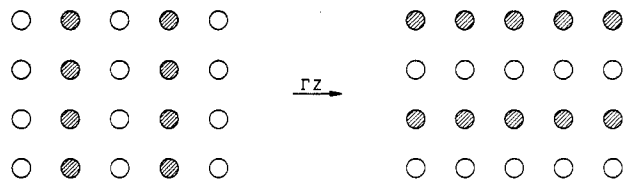

36

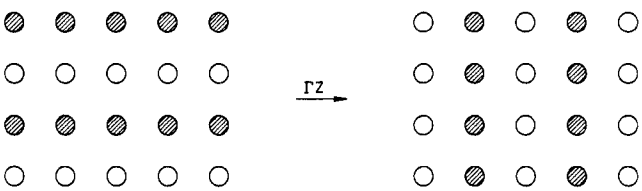

37

According to this band structure the density of states and Fermi level should not be much modified with respect to the two-dimensional layer. This is confirmed by Figure 19, which shows the density of states for two-dimensional and three-dimensional β-PbO. The Fermi level is calculated at −11.27 eV with a gap of 5.90 eV. For that experimental interlayer distance, the overlap populations for the interlayer Pb–Pb bonds are weak: +0.012 for Pb_1–Pb_2 (3.97 Å) and +0.001 for Pb_1–Pb_3 (4.19 Å). This is less

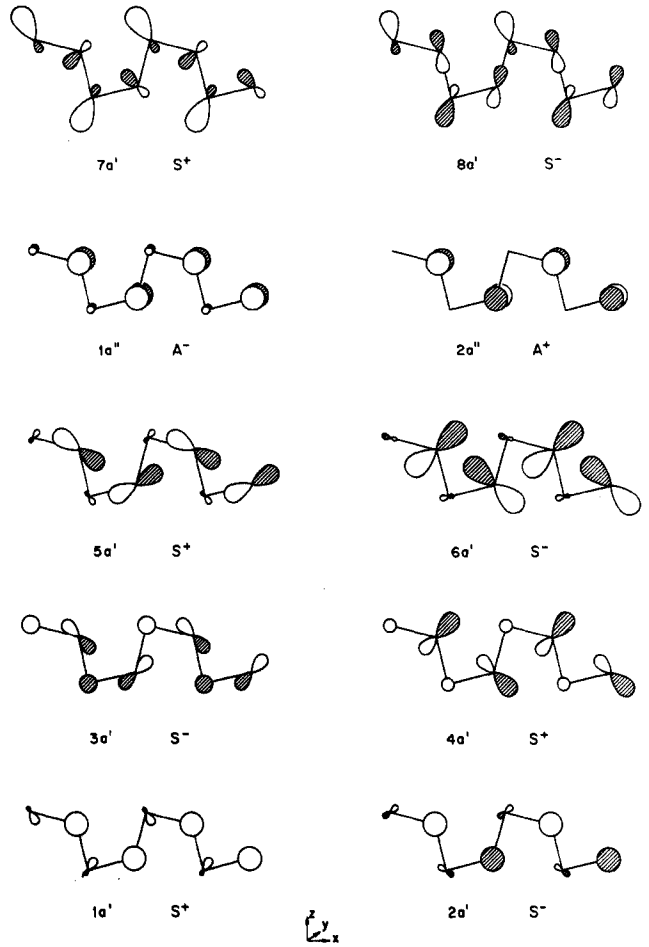

Figure 10. Occupied crystal orbitals of one-dimensional β-PbO chain. Two unit cells are drawn.

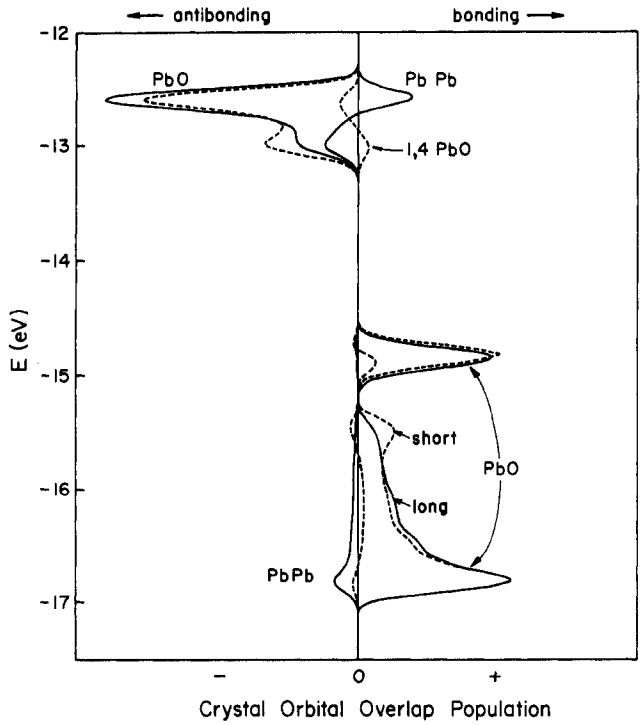

Figure 11. Some COOP curves in the one-dimensional PbO chain.

than in the case of α-PbO (+0.030) but follows simply from the Pb–Pb distance (3.87 Å). The COOP curve for Pb_1–Pb_2 in three-dimensional β-PbO, not given here, has a shape similar to that for the interlayer Pb–Pb bond in α-PbO (Figure 5). There is a typical negative contribution of the top of the valence bands.

TABLE I: Summary of the Overlap Populations and Comparisons with the Force Field Calculated in Ref 17

			d, Å	overlap population	force constant
α	intralayer	Pb–O	2.30	0.116	0.55
		Pb–Pb	3.96	−0.010	0.00
	interlayer	Pb–O	4.32	−0.001	0.00
		Pb–Pb	3.87	0.030	0.40
β	intrachain	Pb–O	2.21	0.155	0.86
		Pb–O	2.22	0.160	0.86
		Pb–Pb	3.86	−0.014	
	interchain	Pb–O	2.49	0.066	0.31
		Pb_1–Pb_4	3.47	0.017	0.10
		Pb_1–Pb_5	3.80	0.034	0.30
		Pb_5–Pb_6	3.63	−0.008	
	interlayer	Pb_1–Pb_2	3.97	0.012	0.62
		Pb_1–Pb_3	4.19	0.001	0.30

The intralayer bonds are not much affected by the layer stacking. This is better shown by considering the motion of the stacking, as we did for α-PbO. Figure 20 displays the evolution of overlap populations when the layers are progressively stacked together. It can be seen that up to the experimental interlayer distance things have not drastically changed: there is only a very small decrease of intrachain (long, vertical) Pb–O and interchain Pb–Pb's. Interlayer Pb_1–Pb_2 is still weak. For shorter interlayer distances, these variations are more pronounced, mainly interlayer Pb_1–Pb_2. Note that interlayer Pb_1–Pb_3 still remains very weak. The energy curve corresponding to this motion is fully repulsive, without any local minimum as for α-PbO. For the experimental geometry, the energy loss due to the stacking is +0.07 eV, which is similar to what was calculated in α-PbO (+0.06 eV). So, for the three-dimensional systems in their experimental geometries, the total energy per PbO unit is still lower, by 0.36 eV, in β-PbO than in α-PbO; this is not in agreement with α-PbO being the lower temperature phase.

Correlation with the Experimental Force Field

A summary of the main overlap populations in three-dimensional α-PbO and β-PbO, in their experimental geometries, is given in Table I. It is tempting to confront these values with other indexes of the bonding in the crystal. Vigouroux, Calvarin, and Husson have performed a normal-coordinate analysis of the vibrational spectra of both phases of PbO.[17] The resulting force constants that they obtained are reported in Table I. As long as we consider intralayer bonds, the correlation is good between our calculated overlap populations and the force constants deduced from the experiment. The interlayer force constants are pretty large, of the same order of magnitude as the intralayer force constant, but they have no real physical meaning. Strong van der Waals interactions between the lone pairs of lead cannot be accounted for satisfactorily by simple "springs" between the lead atoms since quadrupolar interactions are involved. Of course, our method of calculation cannot see reliably the van der Waals interactions either, and gives only weak covalent bonds. Let us emphasize, however, that interlayer Pb–Pb overlap populations are positive in all cases and that the value for α-PbO is quite significant. This is in agreement with a less easy cleavage in α-PbO than in β-PbO.

Within the layers, the correlation between the overlap populations and the force constants is quite satisfactory, particularly the singular dependence on the distance of Pb_1–Pb_4 and Pb_1–Pb_5 in β-PbO is correctly reproduced. Just how good the overall correlation between Pb–Pb and Pb–O overlap populations and experimental force constants is may be seen in Figure 21.

It is worthwhile at this point to state explicitly that we believe there is real but weak Pb–Pb bonding, not just van der Waals forces, between PbO slabs in both modifications of this substance. Extended Hückel calculations cannot and do not simulate van der Waals attractions. On the other hand, they capture the essence of real bonding interactions, even if they sometimes do not re-

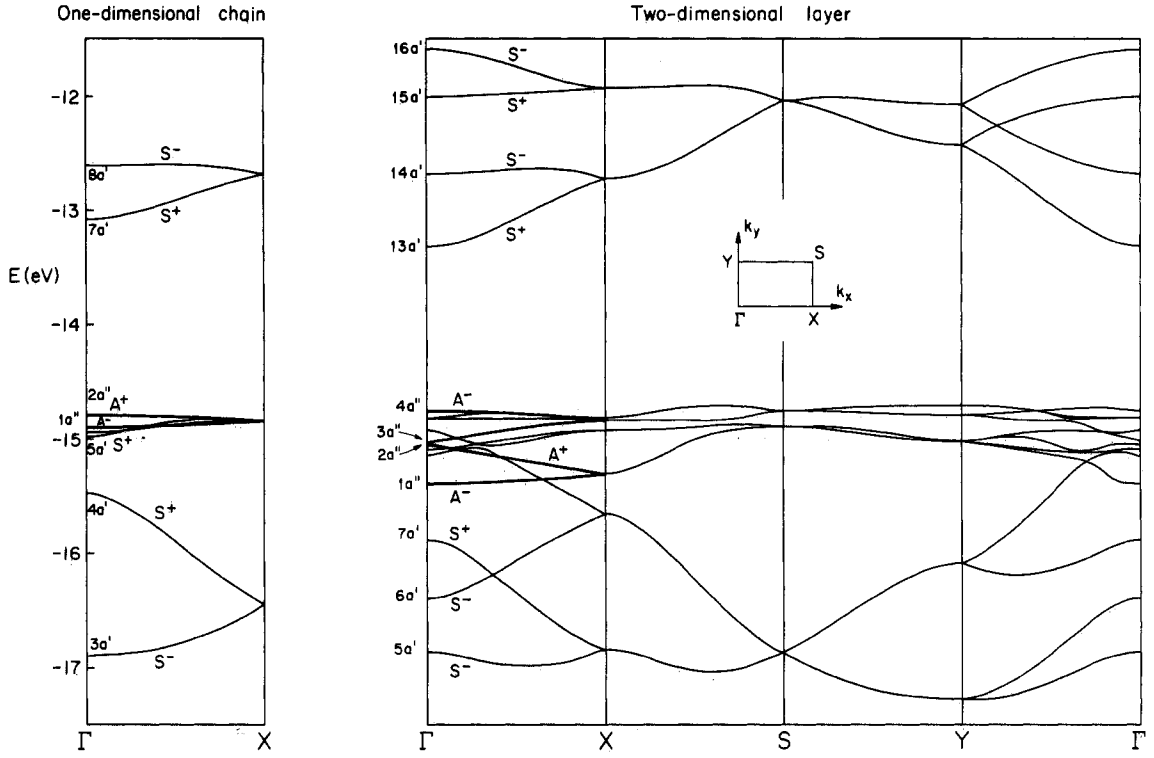

Figure 12. Occupied bands of one-dimensional (left) and two-dimensional (right) β-PbO. The inner set around −33 eV is not shown. The thick curves correspond to bands of a″ symmetry on ΓX line.

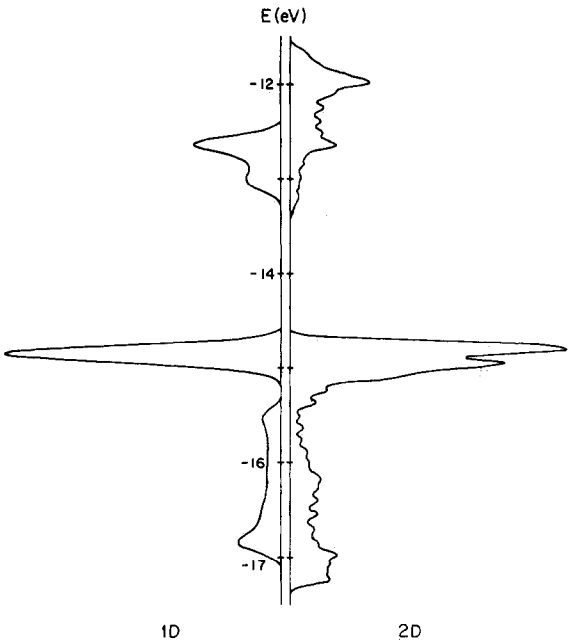

Figure 13. Density of states in a one-dimensional chain (left) and in a two-dimensional layer (right) of β-PbO.

TABLE II: Summary of Fermi Levels and Electronic Gaps Calculated in This Work[a]

	α-PbO		β-PbO		
	2-dimen	3-dimen	1-dimen	2-dimen	3-dimen
Fermi level	−11.62	−10.15	−12.61	−11.60	−11.27
bottom of the conduction band	−3.53	−5.19	−6.30	−5.30	−5.36
electronic gap	8.09	4.96	6.31	6.30	5.90

[a] All values in electronvolts.

produce them quantitatively. The small positive interlayer Pb–Pb overlap populations, together with their increase as the layers are squeezed together, are a clear sign of bonding.

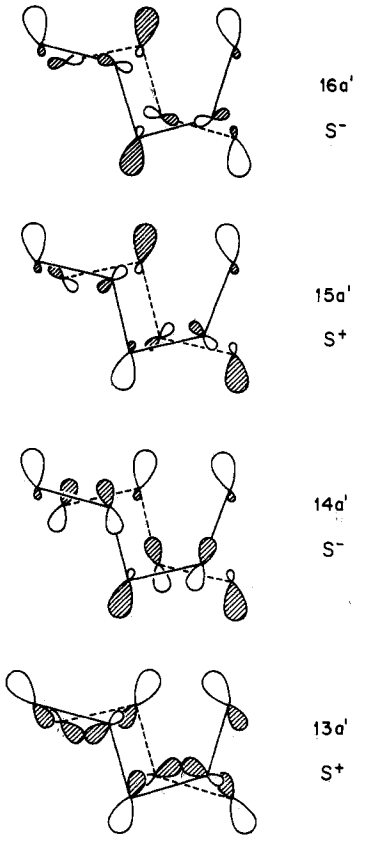

Figure 14. Upper set of occupied crystal orbitals of two-dimensional β-PbO, at the Γ point. One unit cell + one atom are shown.

Electronic Gap

A summary of the gap calculations is given in Table II. The electronic band gaps are known experimentally to be 1.9 eV for α-PbO and 2.5 eV for β-PbO.[4] Our calculated values (4.96 eV for α-PbO and 5.90 eV for β-PbO) are more than twice as large as the experimental ones. Bordovskii et al. calculated the gap at

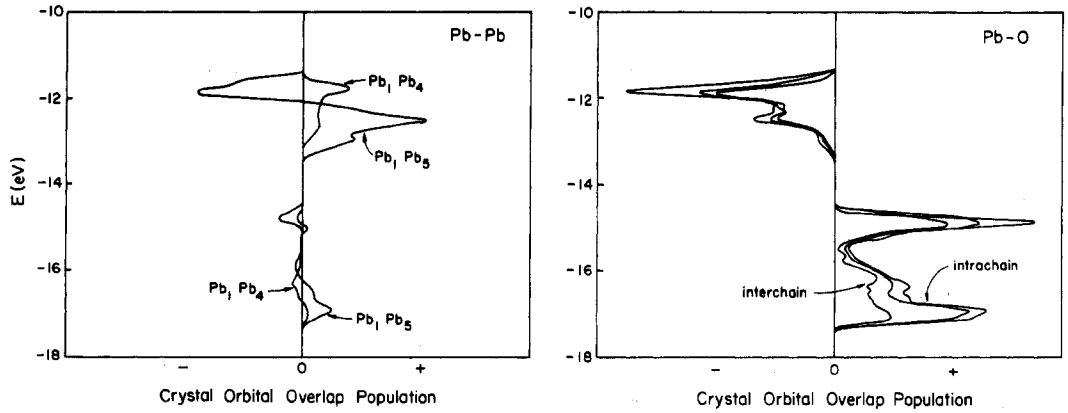

Figure 15. Some COOP curves in the two-dimensional layer of β-PbO. Left: interchain Pb–Pb bonds. Right: Intrachain and interchain Pb–O bonds.

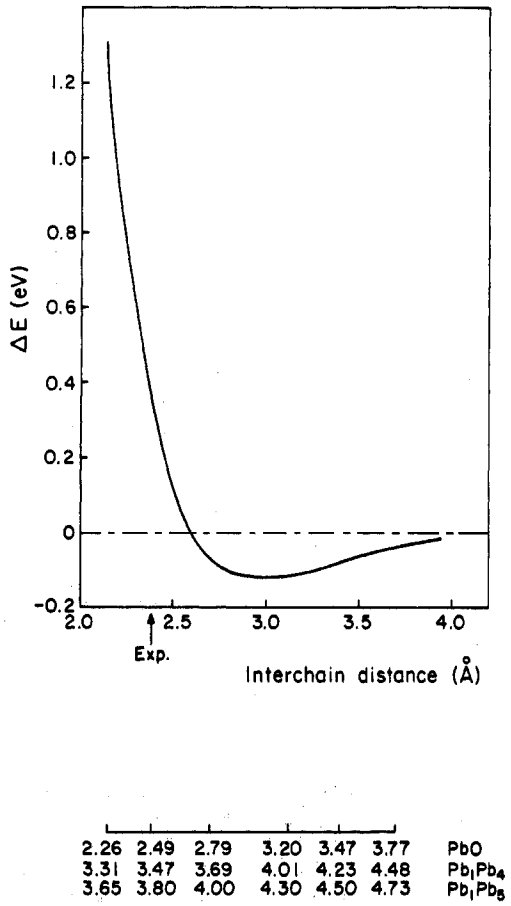

Figure 16. Relative variation of the total energy per PbO unit as a function of the stacking of the chains of β-PbO.

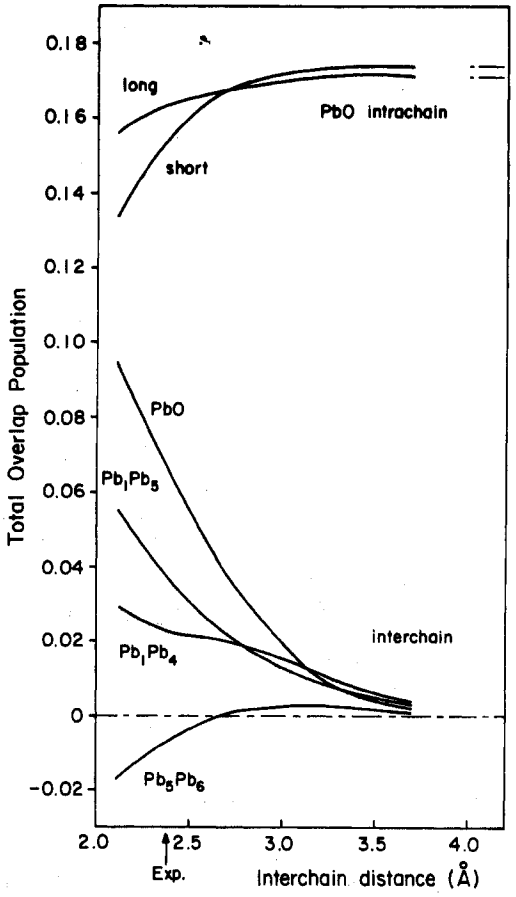

Figure 17. Evolution of some overlap populations as a function of the stacking of the chains of β-PbO.

1.7 eV in α-PbO and 5.7 eV in β-PbO.[15,16] Burdett and Lin calculated an approximate gap of 1.2 eV for α-PbO.[14a] These authors use a method similar to ours but with different parameters. Especially, they use for Pb 6p, $H_{ii} = -9.2$ eV, which is 3 eV lower than the corresponding parameter that we used. Bordovskii et al. use also empirical parameters in their calculation.[15,16] For lead 6p, they took as the valence-state ionization potential a value from Moore's Tables, which is −7.4 eV.[23] In Appendix 2 we report a study of the effects of the choice of parameters on the electronic structure of these compounds. The use of different parameters, in particular those based on nonrelativistic Pb calculations, leads to little change in the bonding but can affect the gap and the density of states. Thus, it is not surprising that the agreement is not good between the various calculations. Maybe our H_{ii} for

TABLE III: Extended Hückel Parameters

orbital	H_{ii}, eV	slater exponent
Pb 6s	−15.41	2.72
Pb 6p	−6.36	1.91
Pb 6s[a]	−12.35	2.38
Pb 6p[a]	−6.90	1.91
O 2s	−32.30	2.275
O 2p	−14.80	2.275

[a] Special "nonrelativistic" set used only in the discussion. See Appendix 2.

Pb 6p (−6.36 eV) is too high in energy, inducing a too high bottom of the conduction band. In agreement with Burdett, we note that in α-PbO the bottom of the conduction band is at the A point (R in ref 14a) in the Brillouin zone ($k_x = k_y = k_z = {}^1/_2$). In Table II, we can see the effect of the stacking on the gap. For α-PbO, the stacking of layers considerably reduces the gap. For β-PbO

(23) Moore, C. E. *Natl. Stand. Ref. Data Ser. (U.S. Natl. Bur. Stand.)* **1971**, *NSRDS-NBS 35*, 208.

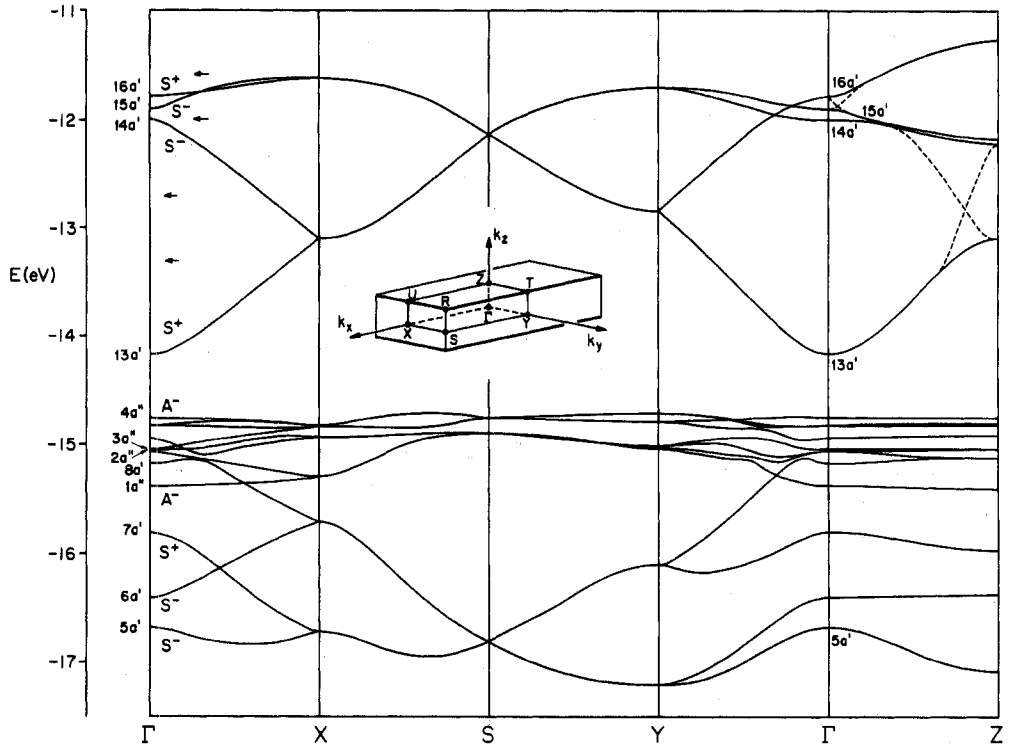

Figure 18. Band structure of three-dimensional β-PbO along five directions of the first Brillouin zone.

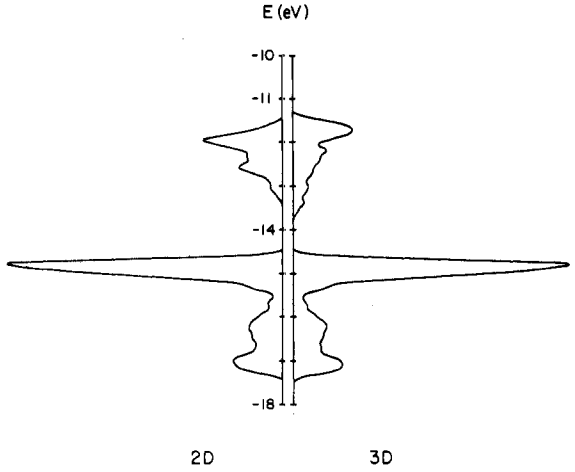

Figure 19. Density of states in β-PbO. Left: two-dimensional layer. Right: Three-dimensional solid.

TABLE IV: Special Point Sets, in Units of $2\pi/a$

	set	no. of k points	definition
			α-PbO
2-dimen	A	36	k_x, k_y = {1/32,3/32,5/32,7/32,9/32,11/32,13/32,15/32}[a]
3-dimen	B	36	A with $k_z = 1/4$
			β-PbO
1-dimen	C	6	k_x = {1/24,3/24,5/24,7/24,9/24,11/24}
	D	20	k_x = {1/80,3/80,5/80,...,39/80}
2-dimen	E	42	k_x = {1/28,3/28,5/28,7/28,9/28,11/28,13/28}
			k_y = {1/24,3/24,5/24,7/24,9/24,11/24}
	F	20	k_x = {1/20,3/20,5/20,7/20,9/20}
			k_y = {1/16,3/16,5/16,7/16}
3-dimen	G	20	F with $k_z = 1/4$

[a] For this square system, weighting factors (1 and 2) are used.

the stacking of chains and of layers reduces the gap little. Bordovskii et al. emphasize that the top of the valence band is mostly on lead.[15,16] In our study it is also mainly on lead but with a certain amount of oxygen, as can be seen in the projections of DOS on lead given in Figure 22. Since the bottom of the conduction band

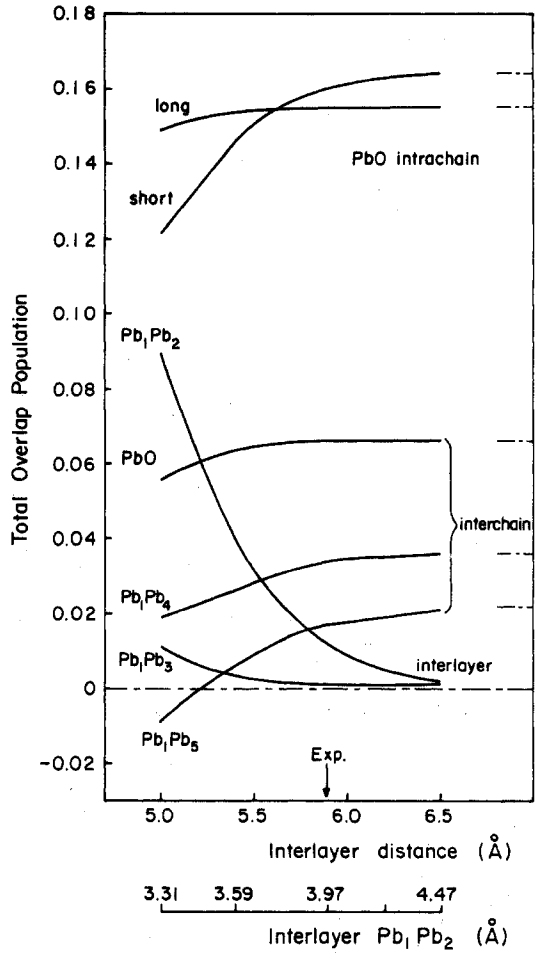

Figure 20. Evolution of some overlap populations as a function of the stacking of the layers of β-PbO.

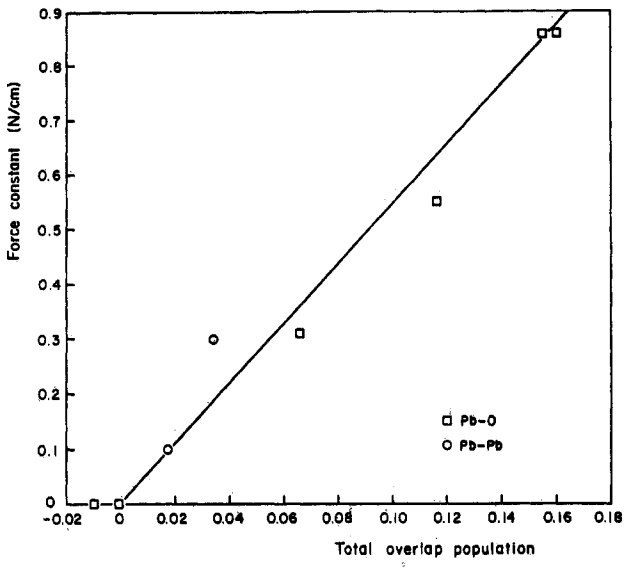

Figure 21. Correlation between calculated intralayer overlap populations and the corresponding force constants deduced from experiment.[17]

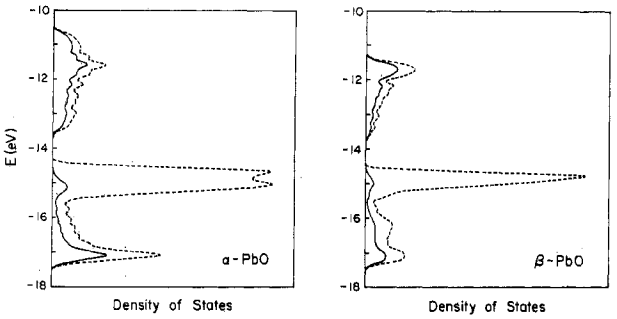

Figure 22. Projection of the density of states on the lead atoms. Full line: Projected DOS. Dashed line: total DOS.

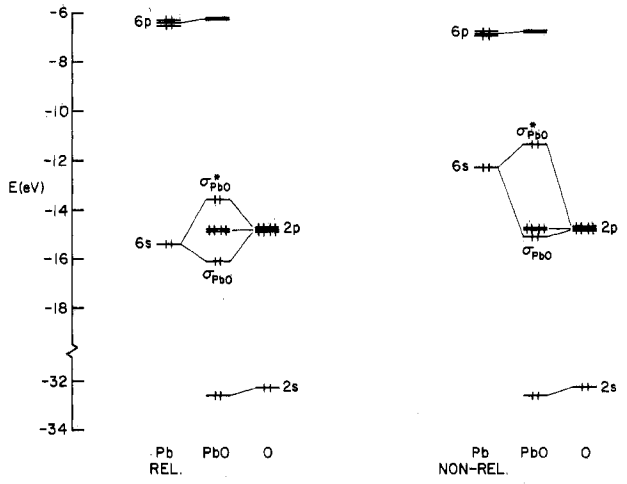

Figure 23. Comparative MO diagrams in diatomic PbO. Left: using relativistic parameters for lead. Right: using nonrelativistic parameters of lead.

is also a mixture of lead and oxygen, we were unable to analyze clearly any eventual charge transfer during electron excitation.

In our calculations, we obtained a substantial net positive charge on lead to which we do not attribute much physical significance. The net charge is nearly the same for α-PbO (+1.57) and β-PbO (+1.60). Thus, we do not confirm the tremendous difference obtained by Bordovskii et al.: +0.00 in α-PbO and +0.89 in β-PbO.[15,16] It is true that they have charge self-consistency in their procedure, whereas we do not in ours. But the two modifications should not be that different, given their geometrical similarity.

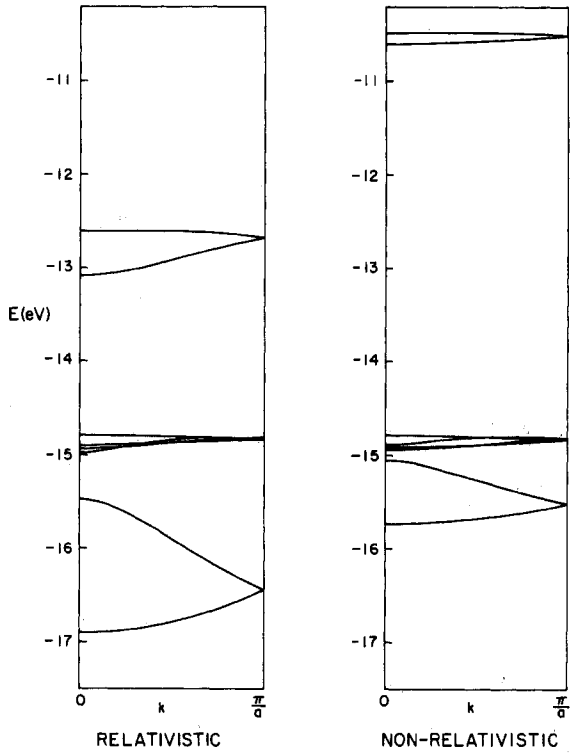

Figure 24. Comparative band structures of one-dimensional β-PbO. Left: relativistic parameters. Right: nonrelativistic parameters.

In conclusion, we think we have shed some light on the bonding in and between the layers of the two varieties of lead monoxide through our analysis of the band structures. We find evidence for stronger interlayer bonding in α-PbO than in β-PbO. We showed that three different chemical bonds hold together the chains in β-PbO. For the intralayer bonding, we support the force fields calculated from experimental vibrational data.

Acknowledgment. We thank Sunil Wijeyesekera and Chong Zheng for their aid and for helpful discussions. The stay of G.T. in Cornell was made possible by a NATO grant for which we are grateful. This work was also supported by the National Science Foundation through research grant CHE 7828048. We thank Jane Jorgensen and Elisabeth Fields for the drawings and Carol Cook for the typing.

Appendix 1

Computational Parameters. The extended Hückel parameters used in this work are listed in Table III. The parameters for lead come from atomic calculations. The main set that was used systematically in our study is taken from ref 24 and is called the "relativistic" parameter set. The "nonrelativistic" set that was used on β-PbO in the discussion is taken from ref 25.

In our calculations, the experimental geometries correspond to the following parameters. α-PbO: Pb–O = 2.300 Å, O–O = 2.800 Å, interlayer Pb–Pb = 3.868 Å. β-PbO: intrachain Pb–O = 2.214 Å and 2.223 Å, ∠O–PbO = 90.4°, ∠PbO–Pb = 120.9°, interchain Pb–O = 2.487 Å, Pb_1–Pb_4 = 3.470 Å, Pb_1–Pb_5 = 3.798 Å, interlayer Pb_1–Pb_2 = 3.973 Å, Pb_1–Pb_3 = 4.186 Å.

For the DOS curves, the COOP curves, the overlap population, and total energy calculations, the summation over the first Brillouin zone is made by using special sets of k points.[26] These are given in Table IV. On β-PbO we have checked that the sets C and D, and E and F, give the same numerical values for energies and overlap populations. Figure 13 is calculated from sets D and E; Figure 19 is computed from sets F and G. In lattice summation,

(24) Desclaux, J.-P. *At. Data Nucl. Data Tables* **1973**, *12*, 311.
(25) McLean, A. D.; McLean, R. S. *At. Data. Nucl. Data Tables* **1981**, *26*, 197.
(26) Chadi, D. J.; Cohen, M. L. *Phys. Rev. B* **1973**, *8*, 5747.

the overlap integrals were set to zero for atoms separated by more than 10.0 Å in α-PbO and 11.7 Å in β-PbO.

Appendix 2

Sensitivity to Lead Parameters. Tne extended Hückel parameters for lead that we used throughout this study were taken from atomic calculations. Because relativistic effects are important for lead,[27] we took our parameters from the relativistic Dirac-Fock calculations by Desclaux.[24] Let us see now what would have been changed in our study of β-PbO if we had started from nonrelativistic calculations such as the Roothan-Hartree-Fock calculations by McLean and McLean.[25] The effects of relativity on atomic parameters are well-known.[27] In lead, relativistic effects contract the 6s orbital and lower its energy (this is known as the inert-pair effect). So, for our parameters this corresponds to an increase of the 6s Slater exponent and of the absolute value of the 6s valence-state ionization potential ($|H_{ii}|$). The 6p atomic level is virtually unchanged (see Table III). Let us redo now our previous analyses using the nonrelativistic parameters for lead. The main difference is therefore that the lead 6s level is now pushed up in energy by about 3 eV. This has two consequences for the bonding in the diatom, as can be seen in Figure 23: (1) the HOMO is higher in energy; (2) the 6s(Pb)-2p(O) energy matching is now not so good so that the "σ_{PbO}" MO's are now quite asymmetrical. The reduced charge matrix gives 1.8 on O for σ_{PbO} and 1.8 on Pb for σ^*_{PbO}.

It follows that in the one-dimensional chain (1) the Fermi level is higher and the gap is reduced since the highest occupied band is pushed up and the lowest unoccupied band (mainly lead 6p) is nearly unchanged, and (2) because of the asymmetrical nature of the two σ_{PbO} MO's, the bands constructed from these MO's should be less dispersed. This is clearly shown in the comparative band structures given in Figure 24. The Fermi level is now at −10.49 eV (vs. −12.61 eV) with a gap of 3.62 eV (vs. 6.30 eV). When the chains are stacked, the energy curve is quite similar to the one occurring with the former parameters (Figure 16): there is a well of 0.15 eV at an interchain distance of ≈3 Å. The variations of overlap populations are not very different from those of Figure 17. The intrachain PbO overlap populations are bigger but this comes from the bonding description in the diatom. Because of the smaller Slater exponent for 6s lead with the nonrelativistic parameters, we have in the diatom a bigger PbO overlap population (0.228 vs. 0.184 with relativistic parameters). The variation of interchain PbO is nearly superposable with the relativistic curve. This is not the case for the Pb-Pb interchain bonds. Although the variations are of the same shape, their values are somewhat larger with the nonrelativistic parameters. At the experimental interchain distance, interchain Pb_1Pb_5 is larger than interchain PbO (0.080 vs. 0.0067). One may relate this to the fact that the set of bands at ≃−14.9 eV, which are quite significantly involved in the interchain bonding (see Figure 15), remain unchanged since they are comprised mainly of oxygen lone pairs. On the other hand, the large overlap population for Pb-Pb interchain bonding may come simply from the small Slater exponent for lead 6s.

When we now stack the layers, the energy curve calculated is more repulsive than that obtained with relativistic parameters. For the experimental interlayer distance, we are at +0.33 eV. The variations of overlap populations have the same shapes, with an early rise of interlayer Pb_1Pb_2, which has the value of 0.031 at the experimental interlayer distance.

So the use of nonrelativistic parameters does not change materially the conclusions concerning bonding in the crystal but does change the band structure and density of states. The dispersion of the highest occupied orbitals, which are more localized on lead, is weak in the direction of the chain (x) but large in the direction of the stacking (z). Finally, the Fermi level is calculated at −6.60 eV (vs. −11.27 eV) with a gap of 1.00 eV (vs. 5.90 eV).

Registry No. PbO, 1317-36-8; Pb, 7439-92-1; O_2, 7782-44-7.

(27) (a) Pitzer, K. S. *Acc. Chem. Res.* **1979**, *12*, 271. (b) Pyykkö, P.; Desclaux, J.-P. *Acc. Chem. Res.* **1979**, *12*, 276.

The Crystal Structure and Molecular Stereochemistry of *trans*-Aquonitrosyl(tetraammine)technetium Dichloride. Correlation of Stereochemistry with Bonding Theory

L. J. Radonovich[1] and J. L. Hoard*

Department of Chemistry, Cornell University, Ithaca, New York 14853 *(Received: June 12, 1984)*

Structure determination for a monoclinic crystal of the title compound provides both the chemical formulation and the detailed stereochemistry of the $[Tc(NO)(NH_3)_4(OH_2)]^{2+}$ ion. The nearly linear TcNO linkage within the complex of effectively C_{4v} geometry conforms to the simplest case of the applicable bonding theory. Tc-OH_2 and averaged Tc-NH_3 distances, 2.168 (4) and 2.164 (5) Å, respectively, represent pure σ-bonding. The dominating role of π-bonding in the TcNO linkage is displayed in the combination of the short Tc-NO distance of 1.716 (4) Å with the relatively long N-O distance of 1.203 (6) Å. Indeed, the observation that this N-O distance is ~0.05 Å longer than the internuclear distance of 1.1507 Å in the free NO(g) molecule has a qualitatively unique interpretation: namely, that the integrated electron density residing in the 2pπ* orbitals of the nitrosyl ligand substantially exceeds that of the single antibonding electron in the neutral NO molecule. Crystal data analysis: A primitive unit cell in $P2_1/m$ containing two ($TcCl_2O_2N_5H_{14}$) has a = 6.858 (2), b = 10.579 (3), c = 6.646 (2) Å, β = 94.01 (2)° (Mo $K\alpha_1$; λ = 0.709 26 Å), with d_{calcd} = 1.968 and d_{exptl} = 1.97 (1) g/mL. Diffracted intensities recorded for $(\sin\theta)/\lambda < 0.774$ Å^{-1} on a FACS-I diffractometer provided a data/parameter ratio of 1886/55 for structure analysis.

I. Introduction

The structure determination for a crystal of the title compound that we report herein was carried out at the request of H. Taube[2] as a means for determining the chemical constitution of the doubly charged cation. Information accompanying submission of the crystals for X-ray diffraction analysis was limited to the specification of the N/Tc ratio as five in the complex and assurance

(1) Present address: Department of Chemistry, University of North Dakota, Grand Forks, ND 58202.

(2) Armstrong, R. A.; Taube, H. *Inorg. Chem.* **1976**, *15*, 1904-9.

0022-3654/84/2088-6711$01.50/0